Inferring Plant Acclimation and Improving Model Generalizability With Differentiable Physics-Informed Machine Learning of Photosynthesis

Aboelyazeed, Doaa
Xu, Chonggang
Gu, Lianhong
Luo, Xiangzhong
Liu, Jiangtao
Shen, Chaopeng

To be published in: Journal of Geophysical Research: Biogeosciences

DOI to publisher's version: 10.1029/2024JG008552

JGR Biogeosciences

RESEARCH ARTICLE
10.1029/2024JG008552

Special Collection:
Advancing Interpretable AI/ML Methods for Deeper Insights and Mechanistic Understanding in Earth Sciences: Beyond Predictive Capabilities

Inferring Plant Acclimation and Improving Model Generalizability With Differentiable Physics-Informed Machine Learning of Photosynthesis

Doaa Aboelyazeed[1], Chonggang Xu[2], Lianhong Gu[3], Xiangzhong Luo[4], Jiangtao Liu[1], Kathryn Lawson[1], and Chaopeng Shen[1]

[1]Civil and Environmental Engineering, The Pennsylvania State University, University Park, PA, USA, [2]Earth and Environmental Sciences Division, Los Alamos National Laboratory, Los Alamos, NM, USA, [3]Environmental Sciences Division, Los Alamos National Laboratory, Oak Ridge National Laboratory, Oak Ridge, TN, USA, [4]Department of Geography, National University of Singapore, Singapore, Singapore

Key Points:

- Learning from A_N, g_S, and $V_{c,max25}$ improved spatial generalization over fewer variables, highlighting the value of multivariate constraints
- Learning acclimation resulted in largely different global A_N from the PFT-only parameterization and even larger PFT-level differences
- Learnable parameters allow A_N, g_S, and $V_{c,max25}$ to be simultaneously captured, reducing their tradeoffs and improving model generalizability

Supporting Information:

Supporting Information may be found in the online version of this article.

Correspondence to:

C. Shen and C. Xu,
cshen@engr.psu.edu;
cxu@lanl.gov

Citation:

Aboelyazeed, D., Xu, C., Gu, L., Luo, X., Liu, J., Lawson, K., & Shen, C. (2025). Inferring plant acclimation and improving model generalizability with differentiable physics-informed machine learning of photosynthesis. *Journal of Geophysical Research: Biogeosciences*, *130*, e2024JG008552. https://doi.org/10.1029/2024JG008552

Received 2 NOV 2024
Accepted 5 JUN 2025

Abstract Net photosynthesis (A_N) is a key component of the global carbon cycle influencing climate feedback over decadal scales. Although plant acclimation to environmental changes can modify A_N, traditional vegetation models in Earth system models (ESMs) often rely on plant functional type (PFT)-specific parameterizations or simplified acclimation assumptions limiting generalizability across time, space, and PFTs. In this study, we developed a differentiable photosynthesis model to learn the environmental dependencies of $V_{c,max25}$ (maximum carboxylation rate at 25°C, representing photosynthetic capacity), as this genre of hybrid physics-informed machine learning can seamlessly train neural networks and process-based equations together. Compared to PFT-specific parameterization of $V_{c,max25}$, learning the environment dependencies of key photosynthetic parameters improved model spatiotemporal generalizability. Applying environmental acclimation to $V_{c,max25}$ led to substantial variations in global mean A_N indicating the need to address acclimation in ESMs. The model effectively captured multivariate observations ($V_{c,max25}$, A_N, and stomatal conductance (g_s)) simultaneously with multivariate constraints, improving generalization across space and PFTs. It also learned sensible acclimation relationships of $V_{c,max25}$ to different environmental conditions. The model explained more than 54%, 57%, and 62% of the variance of A_N, g_s, and $V_{c,max25}$, respectively, presenting a first global-scale spatial test benchmark of A_N and g_s. These results highlight the potential for differentiable modeling to enhance process-based modules in ESMs and effectively leverage information from large, multivariate data sets.

Plain Language Summary Photosynthesis is a major contributor to the global carbon cycle, so any miscalculations can result in large uncertainties. Photosynthesis is described by many parameters, which have been reported to have environmental dependencies (like plant acclimation to environmental changes over time). Here, we used a physics-informed machine learning framework to incorporate these environmental dependencies while learning from a multivariate data set. We found that accounting for plant acclimation can improve model generalizability and impact the simulated photosynthesis rates.

1. Introduction

Photosynthesis is a critical process in regulating the global carbon cycle, serving as one of the largest determinants of carbon exchange between the earth and its atmosphere. It can be significantly influenced by climate change (Konings & Gentine, 2017) due to the direct response of vegetation photosynthesis to atmospheric carbon dioxide levels, temperature, and humidity (Reddy et al., 2010). Current global estimates of carbon fixation through terrestrial photosynthesis (i.e., gross primary productivity, "GPP") rely on various methods and suggest that approximately 120 petagrams (Pg) of carbon are fixed annually (Beer et al., 2010; Friedlingstein et al., 2010; Houghton, 2007). However, recent estimates suggest that this value can be even higher—up to 157 ± 8.5 Pg of carbon per year (Lai et al., 2024). Miscalculation in photosynthesis rates could result in large uncertainty in land carbon cycle predictions under future climate change scenarios (Arora et al., 2020). Such uncertainty can arise from the complex and dynamic ecosystem processes simulated by large-scale land surface models (LSMs), which are a key component in Earth system models (ESMs) used to predict climate responses under different greenhouse emission scenarios (Pietsch & Hasenauer, 2009; H. Wang et al., 2017).

The photosynthesis process can be characterized by multiple parameters as described in the Farquhar model (Farquhar & von Caemmerer, 1982; Farquhar et al., 1980), which is one of the pioneering and most widely-recognized process-based photosynthesis models used in ESMs. These parameters are derived from experimental data that may not be universally applicable across different environmental conditions or plant functional types (PFTs), thus contributing to substantial uncertainty in global photosynthesis simulations (Rogers, 2014). For instance, the maximum carboxylation rate at 25°C ($V_{c,\max 25}$), a key parameter representing plant photosynthetic capacity, has long been regarded as being PFT-dependent. However, recent studies have identified substantial environmental dependencies (Ali et al., 2015; Luo et al., 2021; Smith et al., 2019) highlighting the need for models to better capture these variations.

Multiple approaches have been evolved and implemented in different LSMs employed within ESMs to adequately calibrate different photosynthetic parameters (Spafford & MacDougall, 2021). Among these, the simplest and most traditionally adopted method relies on PFT-specific empirical values (Rogers, 2014). Other methods consider the impact of plant physiological characteristics (e.g., leaf nitrogen content, "LNC," or leaf chlorophyll content) to refine the parameterization (Croft et al., 2017; Dechant et al., 2017; Kattge et al., 2009; Nijs et al., 1995). LNC, in particular, is a key determinant of photosynthetic capacity, as it reflects the availability of Rubisco—the enzyme responsible for carbon fixation (carboxylation) during photosynthesis. Higher LNC typically indicates more Rubisco allocation, leading to higher carboxylation rates and enhanced photosynthetic capacity (Ainsworth & Long, 2005; Hikosaka et al., 2006; Querejeta et al., 2022).

Beyond physiological traits, however, photosynthetic parameters can also exhibit acclimation to environmental conditions. For instance, thermal acclimation (where photosynthetic responses adjust to temperature fluctuations) was reported for $V_{c,\max 25}$ (Ali et al., 2015; Crous et al., 2022; Kattge & Knorr, 2007; Medlyn et al., 2002) as well as for other temperature response function parameters (see Section 2.1). Ecosystem light acclimation occurs in response to short-term fluctuations in incoming radiation (averaged over ∼10 days) as discussed by Luo and Keenan (2020) and references therein (Ali et al., 2015; Crous et al., 2022; Kattge & Knorr, 2007; Medlyn et al., 2002). Day length also plays a key role in the seasonality of photosynthetic activity (Bauerle et al., 2012), as cited in Ali et al. (2015). Elevated CO_2 concentrations significantly impact plant resource-use efficiency and Rubisco activity (Dusenge et al., 2019; Norby & Zak, 2011; Pandurangam et al., 2006), and photosynthetic acclimation and stomatal responses to CO_2 levels have been widely documented in enclosed chamber experiments (Drake et al., 1997) and Free Air CO_2 Enrichment (FACE) studies (Ainsworth & Long, 2005; Ainsworth et al., 2003; Nowak et al., 2004). $V_{c,\max 25}$ has been linked to vapor pressure deficit (Peng et al., 2021) with relative humidity identified as a key factor influencing the photosynthetic capacity parameters (Ali et al., 2015). Moreover, stomatal conductance is directly correlated with vapor pressure deficit: changes in moisture conditions significantly impact stomatal behavior and thus affect both carbon assimilation and transpiration rates (Medlyn et al., 2011; Mott & Parkhurst, 1991).

Despite the growing recognition of these environmental acclimation processes, their integration into models is not widely practiced. Only a few models incorporate some of these dynamics, such as the leaf utilization for nitrogen allocation (LUNA) model (Ali et al., 2016) and an ecological optimality (EO) model (Smith et al., 2019). This EO model is based on the coordination theory, which describes the balance between electron transport and carboxylation process and least-cost hypotheses for investments in carboxylation and water transport capacities.

Besides inadequate representation of acclimation, traditional methods for calibrating photosynthetic parameters in ESMs either aggregate measurements for different PFTs or derive them from a separate model—for example LUNA in version 5 of the Community Land Model (CLM5) (Lawrence et al., 2019). Since $V_{c,\max 25}$ data are normally spatially sparse, they may be biased due to nonsystematic sampling. Given that it is a key parameter that impacts GPP (Massoud et al., 2019), ESMs typically employ further tuning of $V_{c,\max 25}$ to better fit observed GPP values obtained from remote sensing at the global scale, which are based on limited ensemble simulations (e.g., Fisher et al., 2019). However, the parameter calibration process can lead to issues of parameter nonuniqueness (Beven & Freer, 2001), poor spatial generalizability, and low computational efficiency (Tsai et al., 2021).

Due to the limitations of obtaining photosynthesis-related data, it is likely that leveraging multiple observational data sets for different parameters can improve photosynthesis modeling via the effect of data synergy (Fang et al., 2022). For example, leaf gas exchange (LGE) measurements (Gu et al., 2010; Qian et al., 2012; Su et al., 2009) are more abundant and easier to measure compared to photosynthetic capacity (Ely et al., 2021). Existing methods cannot effectively leverage large, multivariate data sets, and simultaneously incorporating

multiple observed variables and data sets is a big challenge due to computational requirements, data co-location limitations (not all variables measured at every location), and the lack of a framework to reconcile differences between variables. For example, multiobjective optimization algorithms (Reed et al., 2012; Vrugt et al., 2003) require extensive simulations, and it would be computationally prohibitive to assimilate data from hundreds of sites.

Machine learning (ML) tools are able to utilize multiple observation sources, scales, and types (Liu et al., 2022, 2023; Song et al., 2024). They can identify complex patterns and make accurate predictions within the confines of their training data, which has been demonstrated for photosynthetic capacity (Luo et al., 2021). However, one of the significant challenges with ML models is the risk of overfitting, where the model becomes too finely tuned to the training data and loses its ability to generalize well to unseen data. This overfitting, as discussed in various applications in hydrology (Liang et al., 2023; S. Wang et al., 2022; Yang et al., 2020), can result in models that perform exceptionally well during training but fail to maintain accuracy in real-world applications and are especially risky to apply to future climate conditions with no historical analogs. Moreover, although ML excels at handling individual data sets, it often struggles to integrate and thread together multiple sets of variables across different processes or scales. This limitation hinders its ability to capture the interconnectedness of various factors in complex systems, underscoring the need for hybrid approaches that combine ML with other modeling techniques to better address these challenges.

Here, we seek an opportunity to support the parameterization and simultaneous reconciliation of photosynthesis models with multivariate observations, assess structural soundness, and learn about plant acclimation to the environment from data without imposing strong assumptions. This opportunity resides within differentiable modeling: a genre of physics-informed machine learning that seamlessly connects neural networks (NNs) and process-based equations, allowing them to be trained together within a unified framework (Bindas et al., 2024; Feng et al., 2022; Shen et al., 2023). "Differentiable" means that the relationships between model inputs and outputs are tracked, and thus their gradients can be obtained efficiently and accurately. NNs provide an adaptive learning capacity by estimating parameters or process representations for the "backbone" physics-based equations. These models can digest large global data sets and output interpretable variables, including those for which training data are not available. In this study, we enhanced a recently-developed differentiable ecosystem model, δ_{psn} (Aboelyazeed et al., 2023), which used an NN to estimate parameters for the Farquhar photosynthesis model (Farquhar et al., 1980; Farquhar & von Caemmerer, 1982). We tested the impact of incorporating plant acclimation to the environment by allowing NNs to learn from various sets of inputs including short-term environmental conditions. We applied multivariate joint training—simultaneously training the model using data for net photosynthesis (A_N), stomatal conductance (g_S), and $V_{c,max25}$—and compared its results to those from models constrained by only two of the variables. We specifically focused on $V_{c,max25}$ due to its significance in photosynthesis modeling and the availability of observational data. However, incorporating additional parameters into the framework is also feasible, offering further opportunities to refine and test different model constraints. Using this multivariate framework, we aimed to address the following research questions:

1. How crucial is considering plant acclimation when predicting the variability of $V_{c,max25}$ and A_N as measured around the world?
2. Can learnable, differentiable photosynthesis models generalize well in space, and how do parameterization choices influence this ability?
3. How valuable is the ability for a global ecosystem model to learn simultaneously from multivariate data sets (i.e., from A_N, g_S, and $V_{c,max25}$)?
4. As more parameters and environmental drivers are incorporated, can the Farquhar photosynthesis model capture all key variables well, or does it introduce tradeoffs among them, which could suggest structural issues?

2. Methods

2.1. Model Description

In this work, we employed a flexible and robust framework capable of learning multiple parameters or functions from multivariable data sets spanning global sites and diverse PFTs, ensuring generalizability. This framework, δ_{psn}, is an enhanced version of a recently developed differentiable photosynthesis model (Aboelyazeed et al., 2023). δ_{psn} is built on two functional pillars (see Figure 1): a neural network module designed to learn

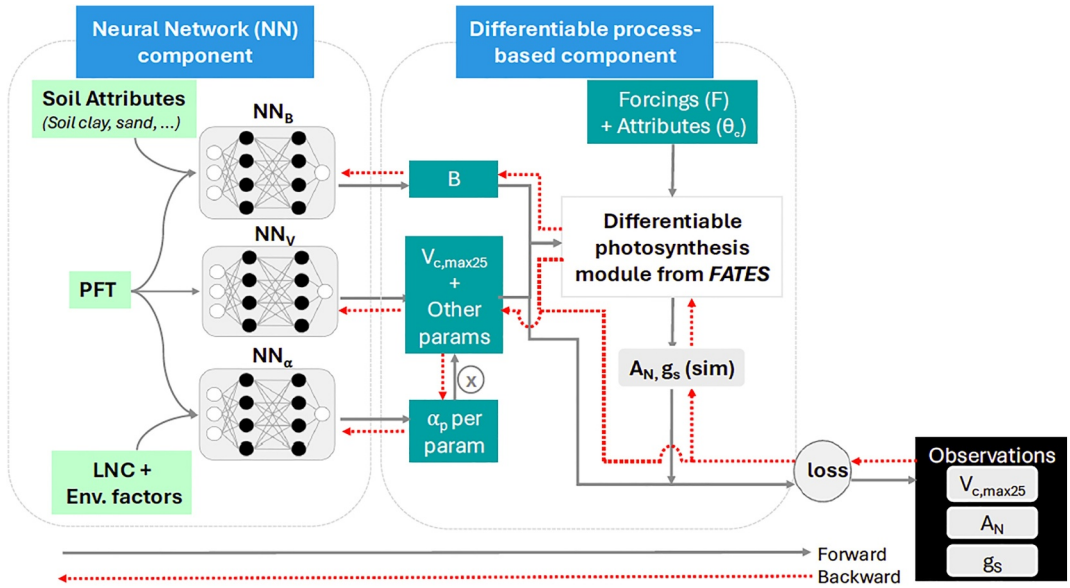

Figure 1. Differentiable ecosystem model (δ_{psn}) framework. The δ_{psn} framework integrates a neural network (NN) component with a differentiable process-based model in this case the photosynthesis module from FATES. The NN component includes three networks—NN_B, NN_V, and NN_α—each trained on different sets of predictors, such as soil attributes, plant functional type (PFT), leaf nitrogen content (LNC), and environmental conditions. These networks learn distinct parameters (including $V_{c,max25}$—the maximum carboxylation rate at 25°C, a key parameter representing plant photosynthetic capacity—and soil water constraint parameter B_i) that feed into the photosynthesis module along with meteorological forcings (F) and constant terrain attributes (θ_c). NN_α captures parameter acclimation to environmental factors, and predicts a perturbation term (α_p) which is multiplied by each parameter (p) learned by NN_V. The photosynthesis module then simulates A_N (net photosynthesis) and g_S (stomatal conductance). The outputs, including $V_{c,max25}$, are compared against multivariate observations to compute a loss function, which guides the backpropagation process to update the NN parameters.

relationships including parameterization schemes from big data, and a physical model based on the leaf-layer photosynthesis module extracted from the Functionally Assembled Terrestrial Ecosystem Simulator (FATES) model (FATES Development Team, 2020). The physics-based photosynthesis module has been reimplemented in PyTorch (Paszke et al., 2017, 2019) so its automatic differentiation engine can ensure programmatic differentiability, which means the ability to rapidly compute gradients of outputs with respect to inputs (models with this ability are termed "differentiable"). An NN module, composed of multiple NNs, maps various observable inputs (such as soil attributes, PFT, LNC, and environmental factors) to physical parameters (including $V_{c,max25}$ and others), which are collectively referred to as θ_p. Unlike purely data-driven supervised machine learning, our approach doesn't require "ground truth" values for θ_p, though they can serve as multivariate constraints when available. θ_p along with meteorological forcings (F, see Section 3) and static attributes (θ_c, any time-static variables or untuned parameters) are then fed into the photosynthesis module, which generates simulations for A_N, g_S, and other intermediate variables. The entire differentiable framework, composed of the differentiable physics-based photosynthesis module and the NN module, is trained using gradient descent in an "end-to-end" fashion (i.e., in a single step) on all training data. This training process minimizes the mismatch between simulated and observed target variables (in this work, A_N, g_S, and/or $V_{c,max25}$), calculated via a "loss function," across the entire training data set.

The neural network module is composed of three NNs: NN_B, NN_V, and NN_α. NN_B learns the soil water constraint parameter B_i (i refers to the particular soil layer), which influences the plant water stress factor β_t (Equation 1a, b). β_t dynamically regulates the plant's photosynthetic capacity based on the soil moisture level in traditional models or is derived from the leaf water potential in more complex ecosystem models simulating plant hydrodynamics (Xu et al., 2023). The computation of β_t from B_i follows the same implementation as in the initial version of δ_{psn} (Aboelyazeed et al., 2023), which is briefly described as:

$$B_i = \mathrm{NN}_B\left(\mathrm{PFT}, \%\mathrm{sand}_i, \%\mathrm{clay}_i, F_{\mathrm{om},i}\right) \quad (1a)$$

$$\beta_t = \Sigma_i f(\Psi_i(B_i, S_i), A)\, r_i \quad (1b)$$

where $\%\text{sand}_i$, $\%\text{clay}_i$, and $F_{\text{om},i}$, respectively, represent the sand percentage, clay percentage, and organic matter fraction of soil layer i. These quantitative variables were integrated with PFT categories, which were transformed into vectors of quantitative variables using an embedding layer in PyTorch or via one-hot encoding—a method that converts categorical input data into quantitative values by mapping each PFT category to a binary vector of zeros and ones (see Table S1 in Supporting information S1, where PFT is represented as a one-hot vector as explained in the Table caption). Ψ_i (mm) is the soil water potential at layer i computed based on B_i and S_i where S_i represents the soil wetness factor derived from soil moisture content at a specific soil layer. r_i represents the plant root distribution factor (Oleson et al., 2013), and A includes other PFT-dependent and soil texture-dependent parameters (refer to Supporting information S1 for more details). Following Aboelyazeed et al. (2023), we used two hidden layers each with a hidden size equal to the number of input features. We applied sigmoid activation functions to both the hidden and output layers with the output layer keeping values between [0–1].

For NN_V, we used two hidden layers with rectified linear unit (ReLU) activation functions and a sigmoid activation function for the output layer. NN_V took the PFT category as the only input predictor, represented via one-hot encoding (see Table S1 in Supporting Information S1), to predict PFT-specific photosynthetic parameters, including $V_{c,\text{max}25}$ (i.e., one predicted parameter value for each PFT). All parameters learned by NN_V, constrained between 0 and 1 using the sigmoid function, were then rescaled to a predefined min-max range based on values from literature (see Table S2 in Supporting information S1). In addition to $V_{c,\text{max}25}$, other predicted parameters included the stomatal slope (g_1) and stomatal intercept (g_0) used in Medlyn's model (Lin et al., 2015; Medlyn et al., 2011), described as:

$$g_s = g_0 + 1.6\left(1 + \frac{g_1}{\sqrt{\text{VPD}}}\right)\frac{A_N \cdot P_{\text{atm}}}{C_s} \quad (2)$$

where g_1 ($\text{kPa}^{0.5}$) reflects the relationship between g_S (μmol m^{-2} s^{-1}) and the assimilation rate, whereas g_0 (μmol m^{-2} s^{-1}) represents the unstressed minimum stomatal conductance, VPD (kPa) is the vapor pressure deficit, C_s (Pa) is the CO_2 partial pressure at the leaf surface, and P_{atm} (Pa) is the atmospheric pressure. g_1 is originally defined in FATES as a PFT-dependent parameter with values defined similar to those used in the Community Atmosphere Biosphere Land Exchange (CABLE) model (De Kauwe et al., 2015), whereas g_0 is assumed to differ based on the plant photosynthetic pathway (i.e., C_3 or C_4; see Table S2 in Supporting information S1). Though g_0 and g_1 are often assigned constant values per PFT, these parameters have been shown to respond to environmental variation. g_1 has been found to vary across PFTs with long-term environmental drivers such as growth temperature (De Kauwe et al., 2015; Lin et al., 2015; Medlyn et al., 2011), mean annual precipitation (Franks et al., 2018), and soil water availability in crops (Ding et al., 2022). Along with long-term adaptation, several studies have reported short-term variability in g_1. Davidson et al. (2023) observed diurnal variations in g_1, and other studies have linked such variation to dynamic changes in relative humidity and CO_2 (G. Katul et al., 2009; G. G. Katul et al., 2009). Seasonal shifts in g_1 have also been linked to changes in temperature, vapor pressure deficit, atmospheric pressure, and CO_2 in some crop species (Li et al., 2022) as well as to leaf water potential in some desert species (Bai et al., 2022). We argue that parameterizing g_1 based on PFT and short-term environmental conditions can capture its seasonal variability as demonstrated in previous studies and avoid inaccuracies associated with assuming fixed g_1 values under seasonally variable conditions (Bai et al., 2022). For g_0, although it is studied less than g_1, it has been shown to vary among species and with leaf phenology (Davidson et al., 2023), and to respond to water stress through changes in leaf water potential (Misson et al., 2004). Thus, we also parameterize g_0 based on PFT and short-term environmental conditions to reflect the impact of PFT-level differences and potentially additional environmental drivers on g_0. This is consistent with the view that g_0, which represents conductance when A_N approaches 0, should not be assumed constant, as zero assimilation can occur under a variety of environmental conditions (Duursma et al., 2019; Miner & Bauerle, 2017). Davidson et al. (2023) further demonstrated that incorporating diurnal variation in g_0 significantly improved transpiration simulations.

NN_V was also set to learn the $V_{c,\text{max}25}$ activation energy parameter (ΔH_a), which is used in the temperature response function (Oleson et al., 2013) to describe the dependency of $V_{c,\text{max}25}$ on leaf temperature (T_l):

$$V_{c,\max} = V_{c,\max 25} \frac{1 + \exp\left(\frac{298.15\Delta S - \Delta H_d}{298.15 \times 0.001\, R_{\text{gas}}}\right)}{1 + \exp\left(\frac{\Delta S T_l - \Delta H_d}{0.001 R_{\text{gas}} T_l}\right)} \exp\left(\frac{\Delta H_a}{298.15 \times 0.001\, R_{\text{gas}}}\left(1 - \frac{298.15}{T_l}\right)\right) \quad (3)$$

where ΔS (J mol^{-1} K^{-1}) is the entropy term, ΔH_a (J mol^{-1}) is the activation energy, ΔH_d is the deactivation energy (J mol^{-1}), R_{gas} is the universal gas constant (8.314 J K^{-1} kmol^{-1}), and T_l (K) is the leaf temperature. In FATES, ΔH_a is assigned a static value, though it has been reported to respond differently to different PFTs, species, and growth temperatures (Kattge & Knorr, 2007; Kumarathunge et al., 2019; Leuning, 2002; Medlyn et al., 2002).

NN_α was employed to capture parameter acclimation to environmental factors. It predicts a perturbation term (α_p), which is multiplied by each parameter (p) learned by NN_V. This modulation allows the final parameter values (θ_p) to reflect the environmental dependencies of these parameters. The soil parameter B is excluded from this process, as it is independently learned by NN_B. To prevent excessive deviations, α_p values outside of [0.5–1.5] were penalized (see Equation 8). NN_V and NN_α jointly predict θ_p as:

$$\theta_p = \text{NN}_V(\text{PFT}) \times \alpha_p \quad (4a)$$

$$\alpha_p = \text{NN}_\alpha\,(\text{PFT}, \text{LNC}, T_{\text{air}}, \text{Rad}, \text{VPD}, \text{C}_{\text{CO}_2}, \text{dyL}) \quad (4b)$$

where T_{air} is the air temperature, Rad is the daytime radiation, C_{CO_2} is the CO_2 concentration, dyL is the day length, and LNC is the leaf nitrogen content. Our selection of these inputs was guided by literature identifying key and potential environmental factors influencing some of these parameters as discussed in the introduction (see Section 1). To ensure α_p reflected environmental growth conditions, we averaged the predictors over the 30 days preceding each measurement date in our data set. Although these factors represent short-term environmental conditions, they still capture underlying long-term signals. In our data set, both short-term and long-term conditions (i.e., 30-day vs. 10-year means) were highly correlated (e.g., $R^2 = 0.55$ between $T_{\text{air},30d}$ and $T_{\text{air},10\text{yr}}$, $R^2 = 0.57$ between VPD_{30d} and $\text{VPD}_{10\text{yr}}$, and $R^2 = 0.51$ between Rad_{30d} and $\text{Rad}_{10\text{yr}}$), suggesting that our short-term predictors inherently embed aspects of long-term adaptation.

Using this setup composed of NN_V and NN_α provided better regularization by constraining the model to PFT-dependent value parameters using NN_V, while just perturbing these values based on environmental conditions as predicted by NN_α. Since this approach restricts information flow from certain inputs to certain parameters, it reduces overfitting. Indeed, directly feeding the environmental conditions into NN_V led to large overfitting, as the high flexibility of NN_V allowed it to generate overly-specific, overfitted parameter values.

The differentiable process-based photosynthesis component in δ_{psn} is based on FATES, which implements the Farquhar model (Farquhar et al., 1980) for C_3 plants and the Collatz model (Collatz et al., 1992) for C_4 plants. The model estimates A_N (μmol m^{-2} s^{-1}) by solving a nonlinear system of equations (Equations 5 and 6) with the intercellular leaf CO_2 partial pressure (C_i; Pa) as the unknown. A_N (μmol m^{-2} s^{-1}) is calculated using the gross photosynthetic rate (A_G; μmol m^{-2} s^{-1}) as:

$$A_N = A_G \cdot C_i - R_d \quad (5)$$

$$C_i = C_a - A_N \cdot P_{\text{atm}} \frac{1.4 g_s + 1.6 g_b}{g_s \cdot g_b} \quad (6)$$

where R_d (μmol m^{-2} s^{-1}) is the plant respiration rate, C_a (Pa) is the CO_2 partial pressure near the leaf surface, and g_S and g_b (μmol m^{-2} s^{-1}) are the stomatal and boundary layer conductance, respectively. Table 1 defines the system of equations with further details provided in Text S3 in Supporting Information S1. We leveraged automatic differentiation to obtain the gradients needed for Newton's iteration method, which solves the nonlinear system (for more details, see Aboelyazeed et al., 2023).

To train δ_{psn}, we employed a loss function (Equation 7) defined on multivariable data sets as:

Table 1
Equations Used in the Photosynthesis Module of δ_{psn}

Type	Equations
Solve for gross photosynthesis: $A_G = f(A_c, A_j, A_p)$	$A_c = \begin{cases} \frac{V_{c,\max}(C_i - \Gamma_*)}{C_i + K_c\left(1 + \frac{O_i}{K_o}\right)} & \text{for } C_3 \text{ plants} \\ V_{c\max} & \text{for } C_4 \text{ plants} \end{cases}$ $A_j = \begin{cases} \frac{J_x(C_i - \Gamma_*)}{4C_i + 8\Gamma_*} & \text{for } C_3 \text{ plants} \\ \alpha(4.6\varphi) & \text{for } C_4 \text{ plants} \end{cases}$ $A_P = \left\{ K_p \frac{C_i}{P_{\text{atm}}} \quad \text{for } C_4 \text{ plants} \right\}$
Solve for net photosynthesis (A_N):	$\theta_{cj} A_i^2 - (A_c + A_j) A_i + A_c A_j = 0$ $\theta_{ip} A_G^2 - (A_i + A_p) A_G + A_i A_p = 0$ $A_N = A_G - R_d$
Solve for stomatal conductance (g_S):	$C_s = C_a - \frac{1.4\, P_{\text{atm}} \cdot A_N}{g_b} \geq 1.0\text{e} - 6$ $g_s^2 + b \cdot g_s + c = 0$ $b = -\left(2(g_0 + d) + \frac{(g_1 \cdot d)^2}{g_b \cdot \text{VPD}}\right)$ $c = g_0^2 + \left(2g_0 + d\left(1 - \frac{g_1^2}{\text{VPD}}\right)\right) d$ $d = \frac{1.6 A_N}{C_s / P_{\text{atm}}}$
Solve for a new value for intercellular leaf CO_2 partial pressure (C_i):	$C_i = C_a - A_N \cdot P_{\text{atm}} \frac{1.4 g_s + 1.6 g_b}{g_s \cdot g_b}$

Note. These equations form a nonlinear system that determines the intercellular leaf CO_2 pressure (C_i) across four steps. Starting with an initial C_i value, steps 1 and 2 involve calculating both gross and net photosynthesis rates (A_G and A_N). In step 3, the stomatal conductance (g_S) is computed, and step 4 provides a revised C_i value. Detailed explanations of the variables and parameters involved are available in Text S3 in Supporting Information S1.

$$L = \text{RMSE}(A_{N,\text{obs}}, A_{N,\text{sim}}) + \text{RMSE}(g_{s,\text{obs}}, g_{s,\text{sim}}) + \text{RMSE}(V_{c,\text{max25,obs}}, V_{c,\text{max25,sim}}) + L_{\text{penalty}} \tag{7}$$

$$L_{\text{penalty}} = \lambda \sum_{p=1}^{P} (\text{ReLU}(\alpha_p - 1.5) + \text{ReLU}(0.5 - \alpha_p)) \tag{8}$$

where the first three terms of Equation 7 represent the root mean square error (RMSE; Equation 9) calculated between simulated and observed A_N, g_S, and $V_{c,\text{max25}}$, respectively. To ensure balanced contributions from each target variable, we experimented with different weights and ultimately settled on using equal weights (1) for each term after normalizing all simulations and observations of each target variable. L_{penalty} (Equation 8) was added to constrain the perturbation parameters α_p within the range [0.5, 1.5]. Here, P represents the number of learned parameters, and λ is a hyperparameter weighting the L_{penalty} term (kept at 1.5).

2.2. Experimental Design

To evaluate the impact of acclimation, we conducted three experiments with different predictor sets: (a) PFT (model trained using only the PFT category, without NN_α included in the model configuration at all), (b) PFT + LNC (with LNC added as a predictor with PFT in NN_α to adjust photosynthetic parameters), and (c) PFT + LNC + ENV (with environmental factors T_{air}, Rad, VPD, C_{CO_2}, and dyL added to PFT and LNC in NN_α). PFT + LNC serves as an intermediate case between the other two experiments, resembling how various vegetation models employ empirical (Clark et al., 2011; Knorr, 2000; Raddatz et al., 2007) and mechanistic (Lawrence et al., 2019; Thornton et al., 2005) approaches to model the photosynthetic capacity based on LNC (Rogers, 2014). The addition of ENV further accounts for parameter acclimation to environmental changes across space and time.

The impact of learning additional photosynthetic parameters alongside $V_{c,max25}$ was assessed by comparing model setups δ_{psn1}, δ_{psn2}, δ_{psn3}, and δ_{psn4}. In δ_{psn1}, only soil parameter B and photosynthetic parameter $V_{c,max25}$ were learned, providing a baseline. δ_{psn2} included three possible schemes, each learning B and $V_{c,max25}$ along with one additional photosynthetic parameter: either g_0, g_1, or ΔH_a. Similarly, δ_{psn3} involved three schemes as well, each learning B and $V_{c,max25}$ with two more parameters. For both δ_{psn2} and δ_{psn3}, the results presented in the paper are the average of the three schemes. In δ_{psn4}, we had only one scheme in which B and $V_{c,max25}$ were learned together with g_0, g_1, and ΔH_a representing the most complex configuration. By comparing these setups, we aimed to evaluate the impact of including additional parameters in the learning process. For more detailed information on these setups and the schemes included in each, see Table S3 in Supporting Information S1.

All δ_{psn} models were tested for spatial generalizability by implementing a spatial holdout test in which one site from the LGE data set (see Section 3) was held out of the training data set and used only for testing, whereas the remaining sites were used for training. This was repeated until each LGE site was held out from training and used for testing once. To ensure sufficient representation per PFT, we ensured that all PFTs used in the spatial test were represented by at least 3 sites in the LGE database. All $V_{c,max25}$ observations (see Section 3) were included in training due to the very limited number of observations, and thus we only report training results for $V_{c,max25}$.

Finally, we applied parameter prediction on a global scale generating global simulations of $V_{c,max25}$ and A_N over a 10-year growing season (2011–2020). We assessed the impact of various parameter learning approaches on model predictivity by employing different pretrained models from δ_{psn1} to δ_{psn4} under the three scenarios: PFT, PFT + LNC, and PFT + LNC + ENV.

For all experiments, we used the coefficient of determination (R^2) (Cheng et al., 2014) to evaluate the model's performance as described in Equation 10:

$$\mathrm{RMSE} = \sqrt{\frac{\sum_{m=1}^{M} (\mathrm{SIM}_m - \mathrm{OBS}_m)^2}{M}} \tag{9}$$

$$R^2 = 1 - \frac{\sum_{m=1}^{M} \left| \mathrm{SIM}_m - \mathrm{OBS}_m \right|}{\sum_{m=1}^{M} \left| \mathrm{OBS}_m - \overline{\mathrm{OBS}} \right|} \tag{10}$$

where SIM and OBS, respectively, refer to simulated and observed values for data point m. $\overline{\mathrm{OBS}}$ was the mean of all observations.

3. Data Sets

For A_N and g_S observations, we leveraged diverse LGE measurements obtained worldwide. We incorporated the LGE database (Knauer et al., 2018; Lin et al., 2015), which has over 40 sites spanning the United States, Europe, Asia, and Australia, the LeafWeb data set (Gu et al., 2023), which has six distinct PFTs in both the United States and China, and two LGE data sets obtained from Parque Natural Metropolitano in Panama (Rogers et al., 2022), and the Caxiuana forest in Brazil (Jardine et al., 2020), which are part of the Next Generation Ecosystem Experiments—Tropics (NGEE-Tropics) project. By combining these data sets, we encompassed a total of 10

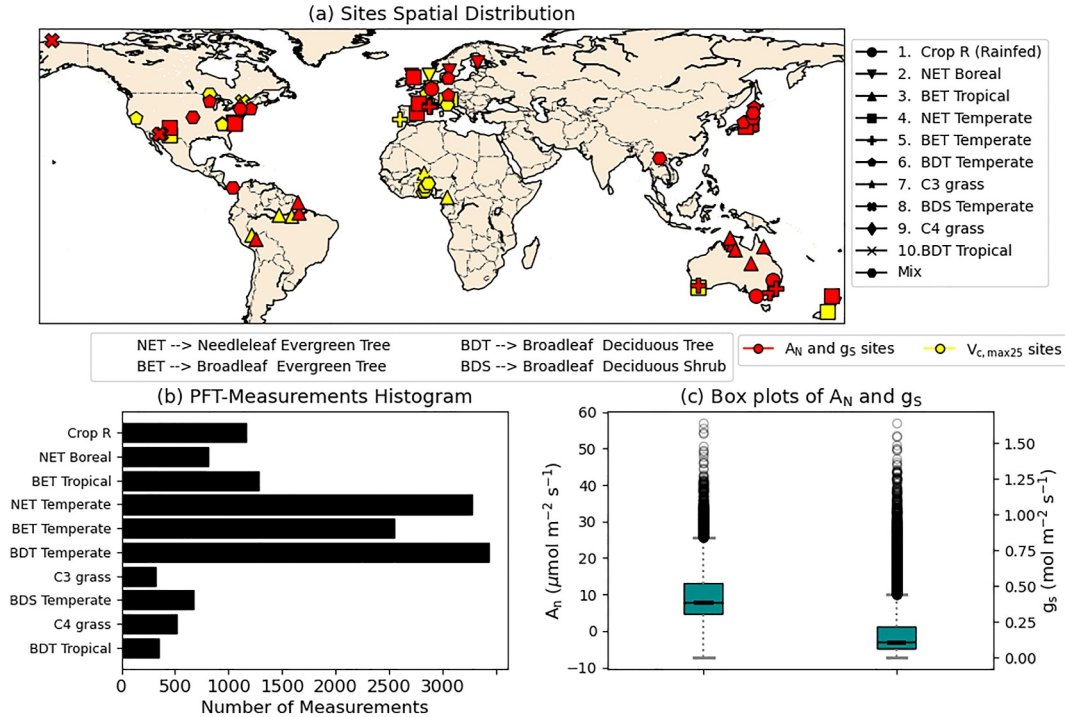

Figure 2. Description of the data used in this study. (a) Spatial map showing the global distribution of study sites, with the symbol shape representing a site's plant functional type (PFT) category, and the color indicating whether the data was from a maximum carboxylation rate at 25°C ($V_{c,max25}$) data set (yellow) or from a leaf gas exchange (LGE) data set (red). (b) PFT measurement histogram showing the number of measurements collected for each PFT, illustrating the distribution and frequency of data across different plant types. (c) Box plots of A_N (net photosynthesis; left box plot and *y*-axis) and g_S (stomatal conductance; right box plot and *y*-axis) observation values across all sites. The central line on each box plot indicates the mean, the top and bottom of the box respectively indicate the 25th and 75th quantiles, and the upper and lower whiskers extend to 1.5 times the interquartile range beyond each edge of the box.

distinct PFTs (see Figure 2a). Among these, the needleleaf evergreen tree (NET), broadleaf evergreen tree (BET), and broadleaf deciduous tree (BDT) temperate PFTs exhibited the highest frequency of measurements (see Figure 2b). A_N values within the data set ranged from −10 to 60 μmol m^{-2} s^{-1} with medians of 10 μmol m^{-2} s^{-1} and 0.1 mol m^{-2} s^{-1} for A_N and g_S, respectively (see Figure 2c). These data sets included instantaneous meteorological forcing data (denoted by F in the top turquoise box in Figure 1) for different sites such as air temperature, leaf temperature, atmospheric pressure, vapor pressure deficit, incoming photosynthetic active radiation, boundary layer conductance, and leaf surface CO_2 concentrations.

Observations of $V_{c,max25}$ were sourced from the same data set as used for the Leaf Utilization of Nitrogen for Assimilation (LUNA) model (Ali et al., 2015, 2016). This data set includes $V_{c,max25}$ observations for 7 PFTs in common with the LGE data sets (excluding Crop R, C_3, and C_4 grass species) spanning around 40 sites around the globe (see yellow points in Figure 2a).

Monthly mean environmental variables (i.e., T_{air}, Rad, VPD, dyL) and LNC linked to A_N, g_S, and $V_{c,max25}$ observations were obtained from the same data sets that included these observations whenever available, whereas missing values were supplemented from other sources (see Table S4 in Supporting Information S1 for a concise summary). For instance, the $V_{c,max25}$ data set (Ali et al., 2015, 2016) contained monthly mean environmental conditions corresponding to each measurement, but the LGE data sets did not. Thus, for LGE sites, we extracted the mean values of the four key factors (T_{air}, Rad, VPD, dyL) over the 30 days preceding each measurement date from the ERA5 Reanalysis data set (Muñoz Sabater, 2019) ensuring consistent temporal aggregation over the sites. ERA5 was selected to fill in the missing variables due to its complete spatial and temporal coverage ensuring consistent data availability across the gap-filled study sites and enabling global simulations. Although we acknowledge potential discrepancies between site-level observations and reanalysis data, we prioritized the originally reported environmental values from Ali et al. (2015) over ERA5 for the $V_{c,max25}$ sites, since they

included values obtained from the original study sources and thus probably better reflected the actual environmental conditions for the $V_{c,max25}$ measurements. Additionally, we found a high correlation between the reported environmental conditions for $V_{c,max25}$ sites from Ali et al. (2015) and the ERA5 data set, confirming a strong alignment between both data sets (data not shown). We used the same approach for LNC, we prioritized values directly reported in the $V_{c,max25}$ data set for these sites. For the LGE sites, following Luo et al. (2021), we used the global leaf nitrogen content (LNC) and specific leaf area (SLA) maps provided by Butler et al. (2017) at a 0.5° resolution to calculate the area-based LNC (gN/m^2). This data set was chosen due to its high performance relative to other LNC products as stated by Luo et al. (2021). To further validate our decision, we tested an alternative data set from Moreno-Martínez et al. (2018) (the second best-performing data set in Luo et al., 2021) and a comparison is provided in Table S5 in Supporting Information S1.

Mean monthly C_{CO_2} (CO_2 concentrations) for LGE and $V_{c,max25}$ sites was sourced from global CO_2 levels recorded at the Mauna Loa Observatory (Keeling et al., 1976). Soil moisture levels at various depths (required for computing the plant water stress factor (β_t); see Text S1 in Supporting Information S1) were also obtained from the ERA5 data set, as it provides data at various soil layers and is available at an hourly resolution, which matches the temporal availability of other instantaneous forcing data associated with A_N and g_S observations. For soil attributes, following Aboelyazeed et al. (2023), we used the percentages of sand and clay from Hengl (2018) and converted soil organic carbon content from Hengl and Wheeler (2018) to soil organic matter using the Van Bemmelen factor of 1.72. These data sets were chosen for their global coverage and multilayer representation ensuring a consistent and comprehensive characterization of soil properties and moisture content across study locations.

For global simulations, essential forcing data and environmental drivers required were extracted from the ERA5 data set between 2011 and 2020 with the months of December, January, and February (DJF) representing the growing season in the southern hemisphere and the months of June, July, and August (JJA) representing the growing season in the northern hemisphere. Globally, all gridded data sets used were scaled to a common resolution of 0.25° (matching ERA5) to minimize discrepancies between them.

4. Results

4.1. Model Evaluations

For $V_{c,max25}$, all models using PFT as the only predictor exhibited poor performance (see the PFT block in Table 2), while the inclusion of LNC as an additional predictor substantially improved model results, and adding ENV further led to a smaller but still noticeable enhancement (see the rightmost column in Table 2). With only PFT as the predictor, all δ_{psn} models explained just ~20% of the $V_{c,max25}$ variance according to the R^2 values. This low variance explained stands in sharp contrast to the PFT + LNC and PFT + LNC + ENV models, which could obtain $R^2 > 0.61$ for $V_{c,max25}$ (see the lower rows of Table 2). Adding LNC (PFT + LNC) explained more than 50% of the $V_{c,max25}$ variability, while incorporating both LNC and ENV (PFT + LNC + ENV) exceeded 60%. This suggests that LNC is a dominant factor, while environmental factors can provide additional refinement. Adding only environmental conditions to PFT (PFT + ENV, see Table S6 in Supporting Information S1) improved $V_{c,max25}$ predictions compared to just PFT but to a lesser extent than PFT + LNC, indicating that LNC is a larger contributor to $V_{c,max25}$ than ENV. Overall, PFT-specific parameterization under-captured the variance by more than 40%, highlighting the substantial influence of additional factors beyond PFT alone. This suggests that although PFT provides a baseline estimate, incorporating other key factors (particularly LNC) must be considered to improve $V_{c,max25}$ estimates. Readers are reminded that the test metrics are for spatial cross-validation while the sample collection dates in general do not overlap, so the metrics reflect the spatiotemporal generalization capability of the model.

As we added LNC or LNC + ENV as predictors, $V_{c,max25}$, A_N, and g_S were much better represented by the model (compare results for each category in Table 2). The R^2 score for A_N (g_S) simulation by δ_{psn1} increased from 0.376 (0.406) in PFT-only models to 0.497 (0.557) in PFT + LNC + ENV models, indicating an overall improvement by over 30%. However, it was noticeable that PFT-only models could perform decently well on A_N and g_S even when there were large errors with $V_{c,max25}$. This highlights the strong modulating roles of parameters other than $V_{c,max25}$. For instance, δ_{psn4} with PFT as the only input and 4 intermediate parameters only had an R^2 of 0.202 for $V_{c,max25}$ but R^2 values of 0.449 and 0.358 for A_N and g_S, respectively. This means each part of the model can be

Table 2
Spatial Test Performance Represented by R^2 Scores of Different Models; Multiple Setups of Differentiable Models Learning an Increasing Number of Parameters From δ_{psn1} to δ_{psn4}

		A_N		g_S		$V_{c,\max25}$
Categories	Model setup	Train	Test	Train	Test	All
PFT	δ_{psn1}	0.546	0.376	0.563	0.406	0.182
	δ_{psn2}	0.568	0.390	0.587	0.393	0.188
	δ_{psn3}	0.581	0.400	0.606	0.369	0.192
	δ_{psn4}	0.606	0.449	0.626	0.358	0.202
PFT + LNC	δ_{psn1}	0.583	0.394	0.605	0.422	0.512
	δ_{psn2}	0.599	0.409	0.629	0.409	0.519
	δ_{psn3}	0.619	0.421	0.658	0.415	0.506
	δ_{psn4}	0.632	0.439	0.671	0.392	0.509
PFT + LNC + ENV	δ_{psn1}	0.683	0.497	0.705	0.557	0.625
	δ_{psn2}	0.691	0.513	0.728	0.560	0.612
	δ_{psn3}	0.698	0.512	0.743	0.539	0.606
	δ_{psn4}	0.703	**0.542**[a]	0.757	0.567	0.615
	$\delta_{psn4}(-g_S)$[b]	0.708	↓0.504	0.527	↓0.380	**↑0.640**[a]
	$\delta_{psn4}(-A_N)$[b]	0.553	↓0.490	0.757	↓0.558	↑0.624
	$\delta_{psn4}(-V_{c,\max25})$[b]	0.720	↓0.514	0.766	**↑0.615**[a]	↓−0.085

Note. Results in the table are classified into three categories, which represent three different learning approaches (see Section 2.2): PFT (trained using only PFT, without NN_α), PFT + LNC (with LNC added as a predictor along with PFT in NN_α to adjust photosynthetic parameters), and PFT + LNC + ENV (with environmental factors added to PFT and LNC in NN_α). [a]Bold values indicate the best-performing configuration for each target variable. [b]Models in all rows except for the last three were trained simultaneously with observations of A_N, g_S, and $V_{c,\max25}$. The last three rows in the table represent δ_{psn4} models with different constraints: trained only on A_N and $V_{c,\max25}$ observations in $\delta_{psn4}(-g_S)$, trained only on g_S and $V_{c,\max25}$ observations in $\delta_{psn4}(-A_N)$, and trained only on A_N and g_S observations in $\delta_{psn4}(-V_{c,\max25})$. For these rows, arrows next to the values indicate the change in performance compared to the PFT + LNC + ENV δ_{psn4} model trained on observations of all three variables (the fourth row from the bottom).

strongly controlled by its parameters to fit its objectives, and thus by tuning other parameters, it can compensate for the errors in $V_{c,\max25}$. This suggests that constraining the system using multivariate observations can better provide physical constraints for the model leading to more robust and reliable predictions. Although it is true that photosynthesis models in the literature can fit to GPP data even when the $V_{c,\max25}$ parameter is only PFT-based, this doesn't necessarily reflect accurate underlying physical processes.

When environmental acclimation was incorporated for other intermediate parameters (the block for PFT + LNC + ENV in Table 2), we obtained substantially better predictability for $V_{c,\max25}$, A_N, and g_S simultaneously without noticeable trade-offs, with model metrics also gradually improving when more intermediate parameters were allowed (Figure 3). The effects of adding LNC and ENV were significant, each time elevating the models to a different level of performance (Figure 3a). However, for both the PFT and PFT + LNC models, increasing the number of learned parameters proved to be more beneficial for A_N than for g_S, indicating a trade-off. For instance, the δ_{psn1} model showed R^2 values of approximately 0.37 for A_N and 0.40 for g_S (see circle markers in Figure 3, left) compared to R^2 values of about 0.45 for A_N and 0.35 for g_S with the δ_{psn4} model. Although adding LNC improved performance moderately over PFT-only models, the same trade-off persisted between A_N and g_S (see square markers in Figure 3, left). Then, when ENV factors were included (PFT + LNC + ENV), we obtained R^2 values of 0.54 for A_N and 0.56 for g_S with the δ_{psn4} model explaining much more of the variance in these two variables. Overall, these results show that environment-dependent acclimation was crucial and had a more substantial impact on model outcomes than merely increasing the number of learned parameters.

With respect to learning from a multivariate data set, we noted a decline in R^2 scores for A_N when δ_{psn4} was trained on only two out of the three target variables (A_N, g_S, and $V_{c,\max25}$) as indicated in the last four rows of Table 2. The

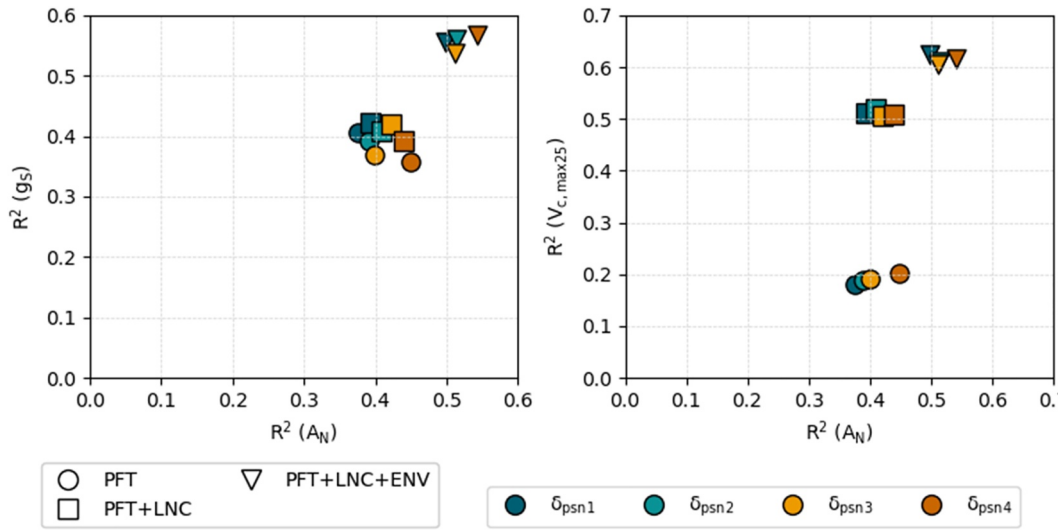

Figure 3. Performance of multiple setups of differentiable models learning an increasing number of parameters from δ_{psn1} to δ_{psn4}. The left plot shows R^2 scores for A_N (net photosynthesis; *x*-axis) versus g_S (stomatal conductance; *y*-axis) simulations. The right plot is the same as the left plot except it shows maximum carboxylation rate at 25°C ($V_{c,max25}$) on the *y*-axis. Different marker shapes represent three different learning approaches: PFT (trained using only plant functional type, without NN_α), PFT + LNC (with leaf nitrogen content added as a predictor along with PFT in NN_α to adjust photosynthetic parameters), and PFT + LNC + ENV (with environmental factors added to PFT and LNC in NN_α). Different colors represent different model setups with an increasing number of parameters learned from δ_{psn1} to δ_{psn4} (see Section 2.2 for details).

most significant decline occurred when A_N was excluded from the loss function, with R^2 declining from 0.542 to 0.490 (refer to $\delta_{psn4}(-A_N)$ in Table 2). A similar trend was noted for g_S, where R^2 decreased when it was not used in training the model (see $\delta_{psn4}(-g_S)$ in Table 2). We found some variations in g_S predictions depending on model constraints. Specifically, the R^2 for g_S was higher when the model was constrained with A_N and g_S compared to when it was constrained with $V_{c,max25}$ and g_S, increasing from 0.558 for $\delta_{psn4}(-A_N)$ to 0.615 for $\delta_{psn4}(-V_{c,max25})$, as shown in Table 2. Conversely, δ_{psn4} demonstrated improved fitting to $V_{c,max25}$ when either A_N or g_S were omitted from the loss function, suggesting that less stringent constraints may benefit the model's performance on specific variables. Notably, $\delta_{psn4}(-V_{c,max25})$ predicted both A_N and g_S decently well despite poor predictions for $V_{c,max25}$, underscoring the critical role of integrating multiple learning objectives to train the model.

4.2. Global-Scale Simulation Comparisons

Plant acclimation has spatially heterogeneous impacts on estimated $V_{c,max25}$ across the globe—increasing the value for some PFTs and decreasing it for others—and the models agreed with the literature for some PFTs (Figure 4). Compared to the PFT-only models, adding acclimation to environmental conditions increased $V_{c,max25}$ in the agricultural lands of India, which was reflected in the values of the rainfed crop PFT (CROP R) having averages of 110 and 140 μmol m^{-2} s^{-1} in PFT-only and PFT + LNC + ENV models, respectively (Figure 5). Adding LNC increased $V_{c,max25}$ in the Southern Hemisphere (Argentina, South Africa, and Southern Australia) where δ_{psn4} for BDS Temperate obtained $V_{c,max25}$ values of 70 μmol m^{-2} s^{-1} with PFT-only models and around 100 μmol m^{-2} s^{-1} with PFT + LNC models. However, when environmental acclimation was introduced (PFT + LNC + ENV), $V_{c,max25}$ decreased again to approximately 80 μmol m^{-2} s^{-1}, bringing the value back closer to the PFT-only estimates. More often, incorporating acclimation to the environment reduced $V_{c,max25}$—for example, (a) across some regions in the U.S. (particularly the Northwest), (b) in central Africa and places with either C_3 or C_4 grass (Figure 5), (c) in NET Temperate zones in the Northern Hemisphere, and (d) in high northern latitudes (compare Figures 4a–4c). Prominent around 60°N, Boreal Forests had a PFT-average $V_{c,max25}$ of 80 μmol m^{-2} s^{-1} for PFT-only models (Figure 4a) compared to values of ~60 μmol m^{-2} s^{-1} in the PFT + LNC and PFT + LNC + ENV models (Figures 4b and 4c), whereas a median value of ~50 μmol m^{-2} s^{-1} was reported by Ali et al. (2015). These regional acclimation adjustments reflect how the data from the sampling sites differed from the PFT-specific mean values. For grasslands, all models recorded the lowest values for C_4 grass with ~20 μmol m^{-2} s^{-1}, but there might be high uncertainty due to the limited available data for grasslands. In the

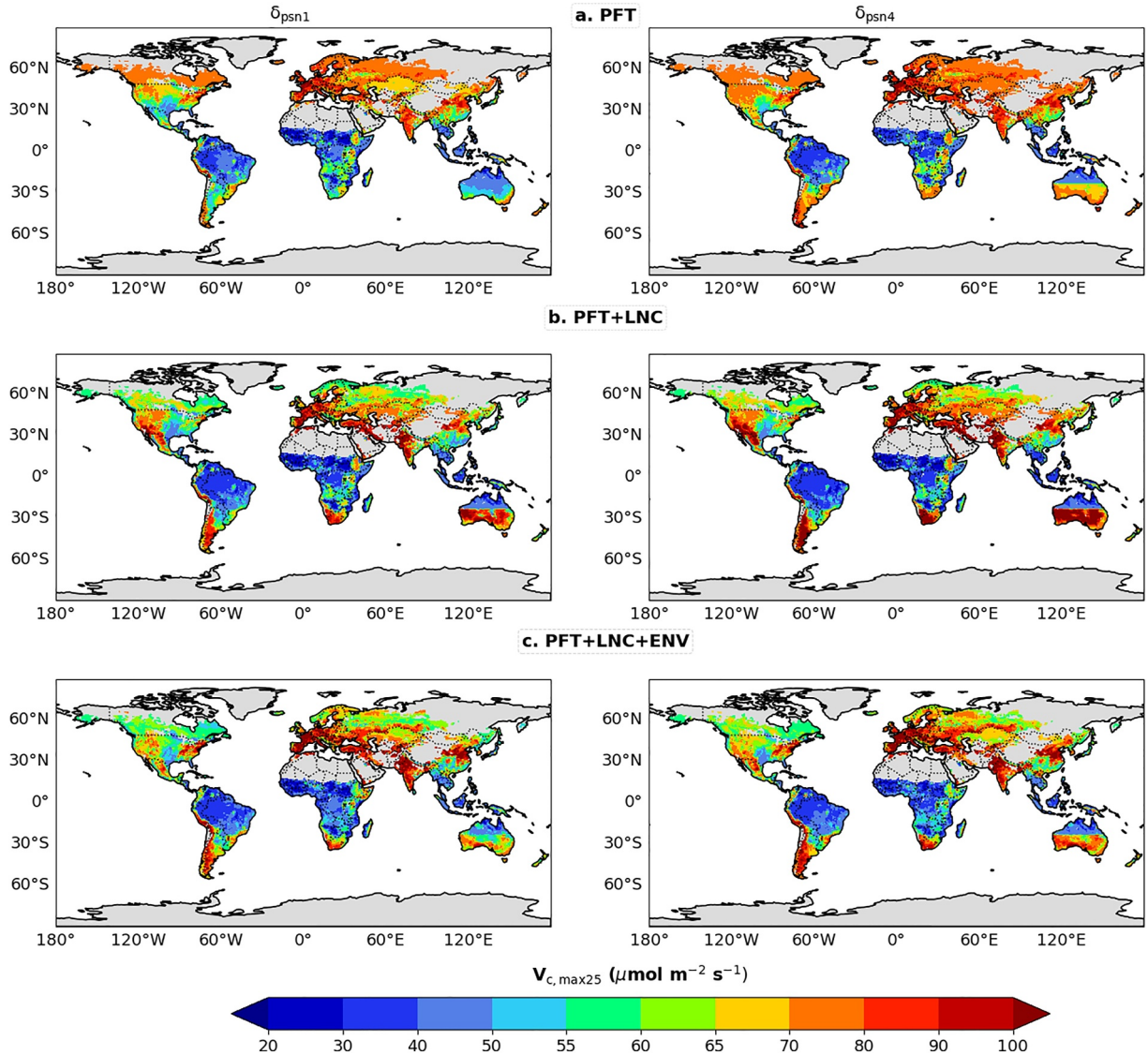

Figure 4. Spatial distribution of global maximum carboxylation rate at 25°C ($V_{c,max25}$) simulations by different sets of models, averaged across a 10-year period (2011–2020) during the growing season (December, January, and February for the Northern Hemisphere and June, July, and August for the Southern Hemisphere). The left (right) column shows simulations by δ_{psn1} (δ_{psn4}) models learning one (four) photosynthetic parameter(s). Different rows represent different learning approaches. The first row (a) shows PFT models, which were trained on plant functional type and did not include NN_{α}. The second row (b) shows PFT + LNC models, where leaf nitrogen content was added as a predictor alongside PFT to NN_{α} to adjust the photosynthetic parameters. The third row (c) shows PFT + LNC + ENV models, where environmental factors were added alongside PFT and LNC as inputs to NN_{α}.

equatorial forests of Africa and the Amazon, low $V_{c,max25}$ values—ranging from ~30 to 45 μmol m^{-2} s^{-1} for BET Tropical and BDT Tropical forests (Figure 5)—were simulated by all models.

Temporally, considering acclimation in the PFT + LNC + ENV case led to seasonal variations in the $V_{c,max25}$ predictions, as depicted by δ_{psn4} model outputs with varying degrees of seasonality observed across different regions across the globe (see Figure S1 in Supporting Information S1). In the Southern Hemisphere, particularly in Argentina, Chile, and South Africa, $V_{c,max25}$ peaked between October and February and exceeded 90 μmol m^{-2} s^{-1}, while during the winter (April-July), values dropped to 70–80 μmol m^{-2} s^{-1} or even lower. Gradually moving north toward the tropics, such as in Central African forests and the Amazon, seasonality was less obvious with $V_{c,max25}$ values remaining relatively stable between 20 and 45 μmol m^{-2} s^{-1} throughout most of the year. In the Northern Hemisphere, seasonal variability was more distinct: (a) Between 0 and 30°N, agricultural lands in India exhibited peak $V_{c,max25}$ between June and September exceeding 90 μmol m^{-2} s^{-1} in western India

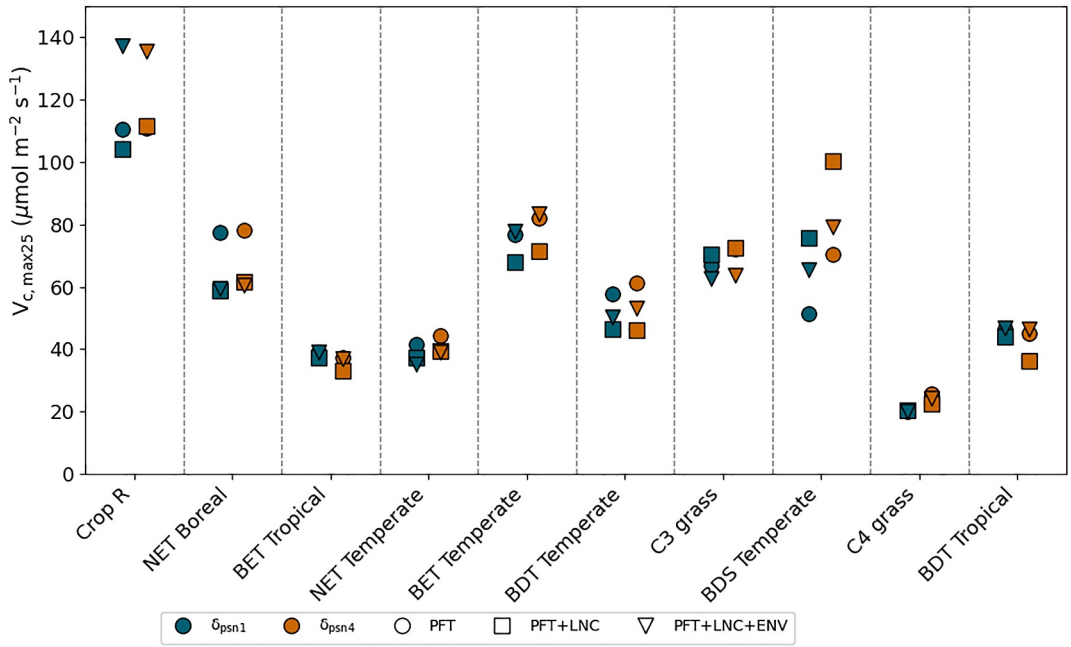

Figure 5. Plant functional type (PFT)-averaged global-scale simulations for global maximum carboxylation rate at 25°C ($V_{c,max25}$) by different sets of models across a 10-year period (2011–2020) during the growing season (December, January, and February for the Northern Hemisphere and June, July, and August for the Southern Hemisphere). Different colors represent different model setups: δ_{psn1} in dark cyan, and δ_{psn4} in dark orange. Different markers represent different learning approaches—PFT models were trained on PFT category and did not include NN_{α}; PFT + LNC models had leaf nitrogen content and PFT as inputs to NN_{α} to adjust photosynthetic parameters; PFT + LNC + ENV models had environmental factors added alongside PFT and LNC as inputs to NN_{α}.

and Pakistan, whereas lower values were generally observed for the rest of the year specifically in eastern India (see light green shades between October to March in Figure S1 in Supporting Information S1). Meanwhile, southeastern China displayed pronounced seasonality with $V_{c,max25}$ values as low as 40–50 μmol m^{-2} s^{-1} from January to March, peaking in June and July, before declining again from September till the end of year. (b) At midlatitudes (just above 30°N), regions in Europe, Turkey, and central Russia reached peak $V_{c,max25}$ values between May and August, followed by a decline in later months. In the southeastern US, $V_{c,max25}$ exhibited a gradual increase starting in March (appearance of orange shades in Figure S1 in Supporting Information S1), peaking from June to August, before declining to its minimum during the winter season of December through February. (c) At higher latitudes (~60°N and higher), the growing season extended from May to November, with values starting around 60 μmol m^{-2} s^{-1} at the beginning of the season, reaching 80 μmol m^{-2} s^{-1} or higher during June and July in some regions in Canada, Russia, Finland, and Sweden before declining again in September and October.

Learning trait variation and acclimation to environmental conditions had an important impact on global-average photosynthesis estimates. Although they both globally reduced simulated net photosynthesis, the effects of LNC and ENV moderately opposed each other. The behavior of δ_{psn} models informed by LNC tended to reduce A_N, while adding ENV partially offset this effect, albeit not fully canceling the influence of LNC (Figure 6). The difference between PFT-only and PFT + LNC + ENV models was moderated when a model with more learned physical parameters like δ_{psn4} was employed. Presumably, the moderation was due to parameter compensation where the more flexible δ_{psn4} model dampened the bias introduced by the PFT-only parameterization of $V_{c,max25}$.

Furthermore, the impact of acclimation in the PFT + LNC + ENV case was obvious when examining seasonal variations compared to PFT-only models. As shown in Figure S2 in Supporting Information S1, considering acclimation played a crucial role in reflecting seasonal fluctuations in the $V_{c,max25}$ predictions and consequently the A_N simulations. Without acclimation, PFT-only models in some regions underestimated $V_{c,max25}$ and led to corresponding underestimations in A_N simulations, particularly during the growing season (e.g., Daintree Forest in Australia—see the top two plots in Figure S2 in Supporting Information S1). Even in regions where seasonality

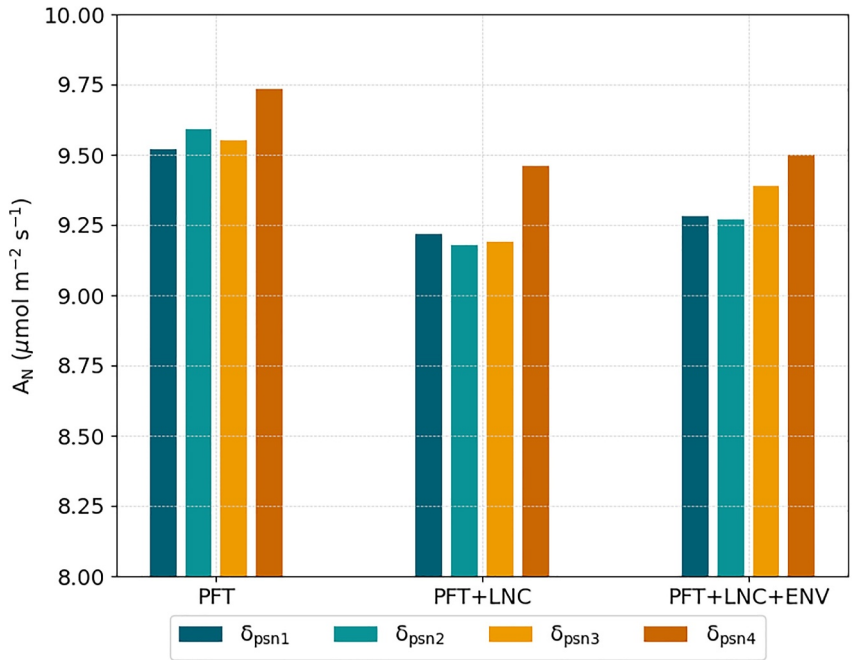

Figure 6. Mean global-scale simulations for net photosynthesis (A_N) by different sets of models across a 10-year period (2011–2020) during the growing season (December, January, and February for the Northern Hemisphere and June, July, and August for the Southern Hemisphere). Different colors represent different model setups with increasing numbers of learned parameters: δ_{psn1} in dark cyan, δ_{psn2} in light cyan, δ_{psn3} in light orange, and δ_{psn4} in dark orange. The three different learning approaches are shown along the *x*-axis—PFT models were trained on plant functional type and did not include NN_α; PFT + LNC models had leaf nitrogen content and PFT as inputs to NN_α to adjust photosynthetic parameters; PFT + LNC + ENV models had environmental factors added alongside PFT and LNC as inputs to NN_α.

was less pronounced (e.g., French Guiana—see the bottom two plots in Figure S2 in Supporting Information S1), PFT-only models still exhibited noticeable discrepancies, overestimating A_N with the absence of acclimation effects.

4.3. Learned Acclimation Relationships

Although we did not constrain the acclimation relationships, the learned relationships largely aligned with expectations despite some limitations due to uncertainties (Figure 7). As anticipated, positive relationships were

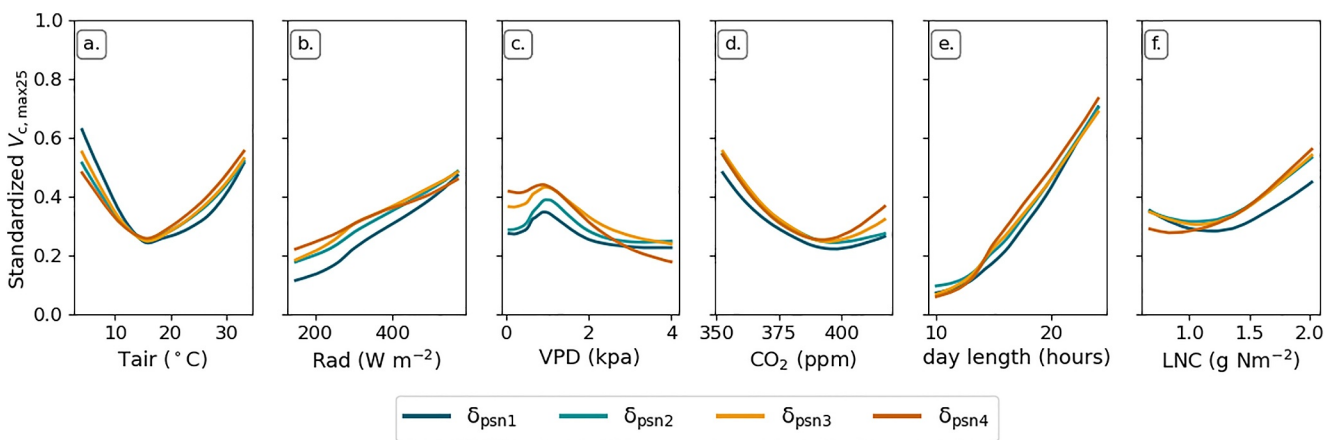

Figure 7. Relationships between learned global maximum carboxylation rate at 25°C ($V_{c,max25}$) and different environmental factors used as predictors, including (a) air temperature, (b) radiation, (c) vapor pressure deficit, (d) CO_2 concentration, (e) day length, and (f) leaf nitrogen content. Different colors represent different model setups with increasing numbers of learned parameters: δ_{psn1} in dark cyan, δ_{psn2} in light cyan, δ_{psn3} in light orange, and δ_{psn4} in dark orange.

spotted between learned $V_{c,max25}$ and daytime radiation (Rad), day length, and LNC by all the models, whereas mostly negative relationships were observed between $V_{c,max25}$ and C_{CO_2} (see Figure 7). More complex relationships also emerged. For example, all models learned a concave-and-then-negative relationship between $V_{c,max25}$ and VPD—increasing until VPD was about 1.0 kPa and then decreasing for higher VPD values (Figure 7c). For temperature, the models exhibited a concave (declining-then-rising) correlation between $V_{c,max25}$ and T_{air}. Interpreting such general trends (despite including some uncertainties) for acclimation can help understand the impact of these short-term environmental factors on plant physiological responses. Additionally, a multimodel approach, as indicated by the multiple lines in Figure 7, provides a broader characterization of these relationships and helps mitigate the influence of potential data artifacts. More details on the implications of these findings are discussed in Section 5.

5. Discussion

$V_{c,max25}$ prediction performance in this study compares favorably to both ML and traditional studies in literature, whereas a comparable benchmark for A_N could not be found. PFT explained only 20% of the variability in $V_{c,max25}$, while adding LNC accounted for approximately an additional 30%. Applying the environmental acclimation to $V_{c,max25}$ further explained over 12% more of its variability, as shown in the PFT + LNC + ENV category (>62% total) in Table 2. Moreover, incorporating environmental acclimation, alongside utilizing different types of observations such as A_N and g_S, substantially improved our models' prediction capabilities for A_N, g_S, and $V_{c,max25}$ collectively (see the last four rows in Table 2). Our results are in agreement with how the importance of environmental acclimation and adaptation has been highlighted in several other studies. For instance, a random forest model trained on leaf traits, annual mean environmental variables, and soil attributes predicted $V_{c,max25}$ with an R^2 of approximately 0.52 (Luo et al., 2021). Similarly, the LUNA model (Ali et al., 2016), which used short-term environmental variables, was able to explain over 55% of the variability in $V_{c,max25}$ for herbaceous plants, trees, and shrubs. With respect to A_N, although some studies in the literature using machine learning have reported R^2 values greater than 0.6, these studies typically assessed A_N for a limited number of species and in a few specific locations rather than globally. These models also used predictors such as leaf morphological traits (Zhang et al., 2020) or vegetation indices derived from remote sensing data (Parida et al., 2024; Wu et al., 2023), which may suggest areas for future model improvement. Hence, our work here established a first global-scale benchmark for A_N, g_S, and $V_{c,max25}$.

Results from Figure 6 suggest that, as previously advocated (Ali et al., 2016; Lombardozzi et al., 2015; Walker et al., 2017), acclimation could have a large impact on the global carbon cycle and needs to be explicitly considered in ESMs. Although the relative differences observed in Figure 6 don't necessarily seem large at face value, they represent a flux term that can be even larger than all global industrial emissions. Fully considering this term has the potential to substantially revise estimates of global carbon fluxes and climate trajectories. In particular, since the PFT-only model is used in most current ESMs, ignoring more realistic parameter representations could be one of several factors contributing to the miscalculation or potential overestimation of A_N. In turn, this could lead to inaccuracies in how these models perform under global warming conditions and contribute to climate models underestimating warming trends. Although this study merely provides an initial investigation into the potential impacts of acclimation, we emphasize that many other factors also influence these climate projections, and our findings should be viewed as one contributing piece within a broader set of uncertainties in ESMs. Here, we provide a unifying framework for incorporating all available observational evidence to better constrain the system dynamics. Nevertheless, our learning approach avoids prescribing precise formulas for relationships or compromising performance if the prescribed relationships introduce biases.

Plant acclimation has been shown in literature to influence global carbon cycle predictions, leading to either higher or lower estimates in different studies. For instance, Lombardozzi et al. (2015) reported that incorporating thermal acclimation of some photosynthetic parameters could increase total ecosystem carbon pools by approximately 25% by 2080. Similarly, Knauer et al. (2023) suggested that current terrestrial biosphere models may underestimate GPP projections by up to 20% under a high-emission scenario (RCP8.5) due to the exclusion of some mechanisms such as photosynthetic thermal acclimation and leaf nitrogen allocation in response to environmental changes. Meanwhile, among various $V_{c,max25}$ parameterizations, using static PFT-dependent values demonstrated the highest GPP trends, compared to parameterizations that accounted for nutrient or environmental scaling (Walker et al., 2017). Additionally, neglecting plant acclimation to environmental changes

could result in an overestimation of the global top canopy leaf layer assimilation (A_N) by approximately 10%–16% under future climate conditions (Ali et al., 2016).

Our findings regarding acclimation relationships highlight key environmental controls on photosynthetic capacity and suggest that differentiable learning frameworks can effectively capture some of these responses. These results have important implications for understanding photosynthetic acclimation and making potential model improvements. The impact of daytime radiation was positive on $V_{c,\max25}$ (see Figure 7), likely because greater light availability enhances plant efficiency and Rubisco activity leading to increased $V_{c,\max25}$, consistent with findings in previous studies (Ali et al., 2015; Peng et al., 2021). Similarly, the positive linear correlation between day length and $V_{c,\max25}$ in δ_{psn} models aligns with findings from Ali et al. (2015), who reported a statistically significant relationship ($p < 0.01$). Conversely, short-term CO_2 concentrations (C_{CO_2}) were negatively correlated with $V_{c,\max25}$, likely due to the effects of carbon fertilization, which can downregulate Rubisco activity under elevated CO_2 concentrations. The concave relationship between $V_{c,\max25}$ and VPD—increasing until around 1.0 kPa before declining (see Figure 7)—is partially consistent with related studies that reported either an increasing relationship between $V_{c,\max25}$ and VPD within a range of ∼0.1–2.7 kPa (Peng et al., 2021) or a decreasing relationship with relative humidity (Ali et al., 2015). For thermal acclimation, existing studies reported diverse relationships between $V_{c,\max25}$ and growth temperature (see Crous et al. (2022) and the references therein) with a negative correlation noted in some studies (Ali et al., 2015; Fürstenau Togashi et al., 2018; Peng et al., 2021). This variability in findings underscores the complexity of thermal acclimation and the variation in species- and biome-level adaptations. Among various environmental factors, studies on thermal acclimation (Kumarathunge et al., 2019) have led to the development and incorporation of multiple temperature response functions into various models (Kattge & Knorr, 2007; Lawrence et al., 2019; Lombardozzi et al., 2015; Luo et al., 2021; Medlyn et al., 2002). On the nutrient side, different models have been used to link photosynthetic capacity ($V_{c,\max25}$) with leaf nitrogen and phosphorus contents (Rogers, 2014; Walker et al., 2017).

Future work could expand hybrid models by incorporating these dynamics, provided sufficient data are available to constrain learning. It should be acknowledged that although our model provides valuable insights, it has inherent limitations, which may cause it to learn compensatory relationships among variables. Overall, the relationships discerned are, unsurprisingly, generally similar to those employed in the mechanistic LUNA model, because they have been both derived from observations. These agreements provide some confidence that the hybrid differentiable learning framework can learn reasonable relationships, if the problem is well posed. However, it is crucial to note the uncertainties regarding these relationships primarily due to the limited number of observational sites. In the future, these uncertainties could be narrowed by incorporating a broader range of data sources, including data for additional variables. Despite these uncertainties, our model's learned $V_{c,\max25}$ values align with the literature for some PFTs. For instance, Ali et al. (2015) reported a median $V_{c,\max25}$ value of ∼80 μmol m^{-2} s^{-1} across temperate ecosystems in the southern hemisphere consistent with the PFT + LNC + ENV estimates from this study (see Figure 5). Additionally, in tropical forests, particularly BET and BDT Tropical ecosystems, our models estimated $V_{c,\max25}$ values below 50 μmol m^{-2} s^{-1}, also aligning with findings from Ali et al. (2015).

This work underscores the remarkable learning capability and flexibility of the differentiable modeling paradigm (Shen et al., 2023; Tsai et al., 2021) to simultaneously learn from multivariate data sets. This approach not only allows for the effective integration of multiple data sets in parameter estimation but also significantly enhances the spatial generalizability of these models. Since the emergence of machine learning models and their introduction to different fields including ecosystem modeling, they have been criticized for not being interpretable and not fully respecting known physical laws and relationships (Rudin, 2019; Shen, 2018). The end-to-end differentiability of this approach allows prior equations to serve as the boundary conditions of neural networks and as the connective tissue between different variables, forcing them to infer specific interpretable relationships. This flexibility to impose questions of interest extends to the components of the loss function (including A_N, g_S, and $V_{c,\max25}$ in our model), as ground truth observations of the learned parameters are not necessarily required.

Nevertheless, we would like to highlight that the learning capacity of the employed NNs within this differentiable paradigm, while inherently flexible, remains constrained by the data sets used for training. The robustness of the results is directly related to the quantity and diversity of the data sets utilized; more extensive and varied data lead to more reliable outcomes (Fang et al., 2022). Specifically, for δ_{psn}, the model is currently constrained by the physics derived from the Farquhar model (Farquhar et al., 1980; Farquhar & von Caemmerer, 1982). Thus, it is

important to improve the data quality and quantity and the flexibility of the mechanistic models for a better predictive understanding of our complex ecosystem processes.

Finally, applying this framework to under-characterized PFTs or regions with scarce observational data remains challenging. Although less data is required than for purely data-driven models, a certain amount is still necessary to ensure generalizability. With limited observations, the model may struggle to extrapolate, leading to high uncertainty. Moreover, ecosystem complexity poses additional challenges, and greater plant trait variability makes it harder to transfer the learned acclimation relationships. Interspecies differences within an ecosystem can lead to over-aggregation, reducing accuracy. Moreover, less extensively studied ecosystems may lack high-quality data, limiting their representation in the training data set and thus effecting model reliability. Therefore, the transferability of such acclimation relationships depends mainly on the quality of the observational data used for model training, their spatial and species coverage, and the specific ecosystem being modeled.

6. Conclusions

In this study, we aimed to enhance global photosynthesis simulations by learning model parameters while incorporating plant acclimation, ultimately to improve land carbon cycle predictions. As expected, plant acclimation to environmental conditions and leaf trait variation demonstrated significant variability in $V_{c,\max 25}$ and A_N for the same plant types across the globe. Models using PFT and LNC accounted for up to 50% of the variability in $V_{c,\max 25}$, whereas the inclusion of additional environmental conditions via learning from A_N, g_S, and $V_{c,\max 25}$ data further increased this percentage. The δ_{psn} models effectively captured acclimation effects without compromising performance across different variables, meaning that the different parts of the model, along with their parameters, each contributed strongly to the simulation of A_N. Considering both plant acclimation and different parameterization schemes could have substantial impacts on global photosynthesis rates and carbon fluxes, with models based solely on PFTs predicting higher rates compared to those that incorporated adaptation to other factors. This point requires further investigation after we incorporate more physical relationships and linkages to more observational constraints. However, our work establishes the first global-scale benchmark for all of these variables and provides a foundation for future model comparisons.

δ_{psn} provides a flexible framework that allows for the simultaneous learning of multiple user-defined parameters from observations across various PFTs and sites, finding formulations that are consistent with the totality of evidence. This adaptability makes it a valuable tool for capturing the complex dynamics of photosynthesis in diverse environmental contexts while inserting modelers' assumptions about which parameters to learn. Looking ahead, there is significant potential for further development of the differentiable ecosystem model, particularly by scaling it up from the leaf level to the whole canopy level. This upscaling would enable the model to learn directly from GPP observations (Pastorello et al., 2020) and thereby enhance its applicability to larger ecosystem processes. Additionally, the δ_{psn} framework could be further expanded by integrating additional modules to simulate other critical ecosystem processes—these developments could occur quickly by leveraging existing experiences from earth system modeling and the learning capability of neural networks.

Conflict of Interest

C.S. and K.L. have financial interests in HydroSapient, Inc., a company, which could potentially benefit from the results of this research. These interests have been reviewed by The Pennsylvania State University in accordance with its individual conflict of interest policy for the purpose of maintaining the objectivity and the integrity of research at The Pennsylvania State University.

Data Availability Statement

The data sets used in the model are available from the sources cited in this paper. The leaf gas exchange databases are publicly accessible: data from Knauer et al., (2018) and Lin et al. (2015) at https://bitbucket.org/gsglobal/leafgasexchange (last accessed: 2024); the leafweb data set (Gu et al., 2023) at https://www.leafweb.org/; and data sets from Jardine et al. (2020) and Rogers et al. (2022) as part of the Next Generation Ecosystem Experiments—Tropics (NGEE-Tropics) at https://ngee-tropics.lbl.gov/research/data/. Observations of $V_{c,\max 25}$ were obtained from Ali et al. (2015, 2016). Global maps of leaf nitrogen content obtained from Butler et al. (2017) and Moreno-

Martínez et al. (2018) are available at https://github.com/abhirupdatta/global_maps_of_plant_traits and https://www.try-db.org/TryWeb/Data.php#59, respectively. Mauna Loa CO_2 records (Keeling et al., 1976) can be accessed at https://gml.noaa.gov/ccgg/trends/. All environmental forcing variables from the ERA5 Reanalysis data set (Muñoz Sabater, 2019) are available through the Climate Data Store at https://cds.climate.copernicus.eu/datasets. Soil texture data (percentages of sand and clay) and soil organic carbon data can be accessed at https://doi.org/10.5281/ZENODO.2525662 (Hengl, 2018) and https://doi.org/10.5281/ZENODO.1475458 (Hengl & Wheeler, 2018), respectively. Figures were created with Matplotlib version 3.8.0 (Hunter, 2007; The Matplotlib Development Team, 2023) available at https://doi.org/10.5281/zenodo.8347255. The differentiable photosynthesis model code is available at [https://doi.org/10.5281/zenodo.15691216] (Aboelyazeed et al., 2025).

Acknowledgments
We thank the data providers for making available the data sets used in this study. We also appreciate the reviewers and editor for their insightful feedback and helpful suggestions. This work was supported primarily by the U.S. Department of Energy, Office of Science, under award number DE-SC0021979. CX acknowledges support through RUBISCO Science Focus Area (SFA) by DOE Office of Science, Biological and Environmental Research (BER) Regional & Global Model Analysis program.

References

Aboelyazeed, D., Xu, C., Gu, L., Luo, X., Liu, J., Lawson, K., & Shen, C. (2025). Inferring plant acclimation and improving model generalizability with differentiable physics-informed machine learning of photosynthesis. https://doi.org/10.5281/zenodo.15691216

Aboelyazeed, D., Xu, C., Hoffman, F. M., Liu, J., Jones, A. W., Rackauckas, C., et al. (2023). A differentiable, physics-informed ecosystem modeling and learning framework for large-scale inverse problems: Demonstration with photosynthesis simulations. *Biogeosciences*, *20*(13), 2671–2692. https://doi.org/10.5194/bg-20-2671-2023

Ainsworth, E. A., & Long, S. P. (2005). What have we learned from 15 years of free-air CO_2 enrichment (FACE)? A meta-analytic review of the responses of photosynthesis, canopy properties and plant production to rising CO_2. *New Phytologist*, *165*(2), 351–372. https://doi.org/10.1111/j.1469-8137.2004.01224.x

Ainsworth, E. A., Rogers, A., Blum, H., Nosberger, J., & Long, S. P. (2003). Variation in acclimation of photosynthesis in Trifolium repens after eight years of exposure to Free Air CO_2 Enrichment (FACE). *Journal of Experimental Botany*, *54*(393), 2769–2774. https://doi.org/10.1093/jxb/erg309

Ali, A. A., Xu, C., Rogers, A., Fisher, R. A., Wullschleger, S. D., Massoud, E. C., et al. (2016). A global scale mechanistic model of photosynthetic capacity (LUNA V1.0). *Geoscientific Model Development*, *9*(2), 587–606. https://doi.org/10.5194/gmd-9-587-2016

Ali, A. A., Xu, C., Rogers, A., McDowell, N. G., Medlyn, B. E., Fisher, R. A., et al. (2015). Global-scale environmental control of plant photosynthetic capacity. *Ecological Applications: A Publication of the Ecological Society of America*, *25*(8), 2349–2365. https://doi.org/10.1890/14-2111.1

Arora, V. K., Katavouta, A., Williams, R. G., Jones, C. D., Brovkin, V., Friedlingstein, P., et al. (2020). Carbon–concentration and carbon–climate feedbacks in CMIP6 models and their comparison to CMIP5 models. *Biogeosciences*, *17*(16), 4173–4222. https://doi.org/10.5194/bg-17-4173-2020

Bai, Y., Liu, Y., Kueppers, L. M., Li, E., Zhang, C., Yu, K., et al. (2022). Hydraulic sensitivity and stomatal regulation of two desert riparian species. *Journal of Geophysical Research: Biogeosciences*, *127*(10), e2022JG006971. https://doi.org/10.1029/2022JG006971

Bauerle, W. L., Oren, R., Way, D. A., Qian, S. S., Stoy, P. C., Thornton, P. E., et al. (2012). Photoperiodic regulation of the seasonal pattern of photosynthetic capacity and the implications for carbon cycling. *Proceedings of the National Academy of Sciences of the United States of America*, *109*(22), 8612–8617. https://doi.org/10.1073/pnas.1119131109

Beer, C., Reichstein, M., Tomelleri, E., Ciais, P., Jung, M., Carvalhais, N., et al. (2010). Terrestrial gross carbon dioxide uptake: Global distribution and covariation with climate. *Science*, *329*(5993), 834–838. https://doi.org/10.1126/science.1184984

Beven, K., & Freer, J. (2001). Equifinality, data assimilation, and uncertainty estimation in mechanistic modelling of complex environmental systems using the GLUE methodology. *Journal of Hydrology*, *249*(1), 11–29. https://doi.org/10.1016/s0022-1694(01)00421-8

Bindas, T., Tsai, W.-P., Liu, J., Rahmani, F., Feng, D., Bian, Y., et al. (2024). Improving river routing using a differentiable Muskingum-Cunge model and physics-informed machine learning. *Water Resources Research*, *60*(1), e2023WR035337. https://doi.org/10.1029/2023WR035337

Butler, E. E., Datta, A., Flores-Moreno, H., Chen, M., Wythers, K. R., Fazayeli, F., et al. (2017). Mapping local and global variability in plant trait distributions. *Proceedings of the National Academy of Sciences of the United States of America*, *114*(51), E10937–E10946. https://doi.org/10.1073/pnas.1708984114

Cheng, C.-L., Shalabh, & Garg, G. (2014). Coefficient of determination for multiple measurement error models. *Journal of Multivariate Analysis*, *126*, 137–152. https://doi.org/10.1016/j.jmva.2014.01.006

Clark, M. P., Kavetski, D., & Fenicia, F. (2011). Pursuing the method of multiple working hypotheses for hydrological modeling. *Water Resources Research*, *47*(9). https://doi.org/10.1029/2010wr009827

Collatz, G., Ribas-Carbo, M., & Berry, J. (1992). Coupled photosynthesis-stomatal conductance model for leaves of C4 plants. *Australian Journal of Plant Physiology*, *19*(5), 519. https://doi.org/10.1071/PP9920519

Croft, H., Chen, J. M., Luo, X., Bartlett, P., Chen, B., & Staebler, R. M. (2017). Leaf chlorophyll content as a proxy for leaf photosynthetic capacity. *Global Change Biology*, *23*(9), 3513–3524. https://doi.org/10.1111/gcb.13599

Crous, K. Y., Uddling, J., & De Kauwe, M. G. (2022). Temperature responses of photosynthesis and respiration in evergreen trees from boreal to tropical latitudes. *New Phytologist*, *234*(2), 353–374. https://doi.org/10.1111/nph.17951

Davidson, K., Lamour, J., Rogers, A., Ely, K., Li, Q., McDowell, N., et al. (2023). Short-term variation in leaf-level water use efficiency in a tropical forest. *New Phytologist*, *237*(6), 2069–2087. https://doi.org/10.1111/nph.18684

Dechant, B., Cuntz, M., Vohland, M., Schulz, E., & Doktor, D. (2017). Estimation of photosynthesis traits from leaf reflectance spectra: Correlation to nitrogen content as the dominant mechanism. *Remote Sensing of Environment*, *196*, 279–292. https://doi.org/10.1016/j.rse.2017.05.019

De Kauwe, M. G., Kala, J., Lin, Y.-S., Pitman, A. J., Medlyn, B. E., Duursma, R. A., et al. (2015). A test of an optimal stomatal conductance scheme within the CABLE land surface model. *Geoscientific Model Development*, *8*(2), 431–452. https://doi.org/10.5194/gmd-8-431-2015

Ding, R., Xie, J., Mayfield-Jones, D., Zhang, Y., Kang, S., & Leakey, A. D. B. (2022). Plasticity in stomatal behaviour across a gradient of water supply is consistent among field-grown maize inbred lines with varying stomatal patterning. *Plant, Cell and Environment*, *45*(8), 2324–2336. https://doi.org/10.1111/pce.14358

Drake, B. G., Gonzalez-Meler, M. A., & Long, S. P. (1997). More efficient plants: A consequence of rising atmospheric CO_2? *Annual Review of Plant Physiology and Plant Molecular Biology*, *48*(1), 609–639. https://doi.org/10.1146/annurev.arplant.48.1.609

Dusenge, M. E., Duarte, A. G., & Way, D. A. (2019). Plant carbon metabolism and climate change: Elevated CO_2 and temperature impacts on photosynthesis, photorespiration and respiration. *New Phytologist*, *221*(1), 32–49. https://doi.org/10.1111/nph.15283

Duursma, R. A., Blackman, C. J., Lopéz, R., Martin-StPaul, N. K., Cochard, H., & Medlyn, B. E. (2019). On the minimum leaf conductance: Its role in models of plant water use, and ecological and environmental controls. *New Phytologist*, *221*(2), 693–705. https://doi.org/10.1111/nph.15395

Ely, K. S., Rogers, A., Agarwal, D. A., Ainsworth, E. A., Albert, L. P., Ali, A., et al. (2021). A reporting format for leaf-level gas exchange data and metadata. *Ecological Informatics*, *61*, 101232. https://doi.org/10.1016/j.ecoinf.2021.101232

Fang, K., Kifer, D., Lawson, K., Feng, D., & Shen, C. (2022). The data synergy effects of time-series deep learning models in hydrology. *Water Resources Research*, *58*(4), e2021WR029583. https://doi.org/10.1029/2021WR029583

Farquhar, G. D., & von Caemmerer, S. (1982). Modelling of photosynthetic response to environmental conditions. In O. L. Lange, P. S. Nobel, C. B. Osmond, & H. Ziegler (Eds.), *Physiological plant ecology II: Water relations and carbon assimilation* (pp. 549–587). Springer Berlin Heidelberg. https://doi.org/10.1007/978-3-642-68150-9_17

Farquhar, G. D., von Caemmerer, S., & Berry, J. A. (1980). A biochemical model of photosynthetic CO_2 assimilation in leaves of C3 species. *Planta*, *149*(1), 78–90. https://doi.org/10.1007/BF00386231

FATES Development Team. (2020). The functionally assembled terrestrial ecosystem simulator (FATES) (Version sci.1.35.5_api.11.0.0) [Computer software]. *Zenodo*. https://doi.org/10.5281/zenodo.3825474

Feng, D., Liu, J., Lawson, K., & Shen, C. (2022). Differentiable, learnable, regionalized process-based models with multiphysical outputs can approach state-of-the-art hydrologic prediction accuracy. *Water Resources Research*, *58*(10), e2022WR032404. https://doi.org/10.1029/2022WR032404

Fisher, R. A., Wieder, W. R., Sanderson, B. M., Koven, C. D., Oleson, K. W., Xu, C., et al. (2019). Parametric controls on vegetation responses to biogeochemical forcing in the CLM5. *Journal of Advances in Modeling Earth Systems*, *11*(9), 2879–2895. https://doi.org/10.1029/2019ms001609

Franks, P. J., Bonan, G. B., Berry, J. A., Lombardozzi, D. L., Holbrook, N. M., Herold, N., & Oleson, K. W. (2018). Comparing optimal and empirical stomatal conductance models for application in Earth system models. *Global Change Biology*, *24*(12), 5708–5723. https://doi.org/10.1111/gcb.14445

Friedlingstein, P., Houghton, R. A., Marland, G., Hackler, J., Boden, T. A., Conway, T. J., et al. (2010). Update on CO_2 emissions. *Nature Geoscience*, *3*(12), 811–812. https://doi.org/10.1038/ngeo1022

Fürstenau Togashi, H., Prentice, I. C., Atkin, O. K., Macfarlane, C., Prober, S. M., Bloomfield, K. J., & Evans, B. J. (2018). Thermal acclimation of leaf photosynthetic traits in an evergreen woodland, consistent with the coordination hypothesis. *Biogeosciences*, *15*(11), 3461–3474. https://doi.org/10.5194/bg-15-3461-2018

Gu, L., Grodzinski, B., Han, J., Marie, T., Zhang, Y.-J., Song, Y. C., & Sun, Y. (2023). An exploratory steady-state redox model of photosynthetic linear electron transport for use in complete modelling of photosynthesis for broad applications. *Plant, Cell and Environment*, *46*(5), 1540–1561. https://doi.org/10.1111/pce.14563

Gu, L., Pallardy, S. G., Tu, K., Law, B. E., & Wullschleger, S. D. (2010). Reliable estimation of biochemical parameters from C3 leaf photosynthesis–intercellular carbon dioxide response curves. *Plant, Cell and Environment*, *33*(11), 1852–1874. https://doi.org/10.1111/j.1365-3040.2010.02192.x

Hengl, T. (2018). Sand content in % (kg/kg) at 6 standard depths (0, 10, 30, 60, 100 and 200 cm) at 250 m resolution (Version v0.2) [Dataset]. *Zenodo*. https://doi.org/10.5281/ZENODO.2525662

Hengl, T., & Wheeler, I. (2018). Soil organic carbon content in X 5 G/kg at 6 standard depths (0, 10, 30, 60, 100 and 200 Cm) at 250 M resolution [Dataset]. *Zenodo*. https://doi.org/10.5281/ZENODO.1475458

Hikosaka, K., Ishikawa, K., Borjigidai, A., Muller, O., & Onoda, Y. (2006). Temperature acclimation of photosynthesis: Mechanisms involved in the changes in temperature dependence of photosynthetic rate. *Journal of Experimental Botany*, *57*(2), 291–302. https://doi.org/10.1093/jxb/erj049

Houghton, R. A. (2007). Balancing the global carbon budget. *Annual Review of Earth and Planetary Sciences*, *35*(2007), 313–347. https://doi.org/10.1146/annurev.earth.35.031306.140057

Hunter, J. D. (2007). Matplotlib: A 2D graphics environment. *Computing in Science & Engineering*, *9*(3), 90–95. https://doi.org/10.1109/MCSE.2007.55

Jardine, K., Zorzanelli, R., Gimenez, B., Robles, E., & Rosa, L. (2020). Raw leaf gas exchange data in the Amazon basin. *U.S. Department of Energy Office of Scientific and Technical Information*, 2014–2016. https://doi.org/10.15486/ngt/1602143

Kattge, J., & Knorr, W. (2007). Temperature acclimation in a biochemical model of photosynthesis: A reanalysis of data from 36 species. *Plant, Cell and Environment*, *30*(9), 1176–1190. https://doi.org/10.1111/j.1365-3040.2007.01690.x

Kattge, J., Knorr, W., Raddatz, T., & Wirth, C. (2009). Quantifying photosynthetic capacity and its relationship to leaf nitrogen content for global-scale terrestrial biosphere models. *Global Change Biology*, *15*(4), 976–991. https://doi.org/10.1111/j.1365-2486.2008.01744.x

Katul, G., Manzoni, S., Palmroth, S., & Oren, R. (2009). A stomatal optimization theory to describe the effects of atmospheric CO_2 on leaf photosynthesis and transpiration. *Annals of Botany*, *105*(3), 431–442. https://doi.org/10.1093/aob/mcp292

Katul, G. G., Palmroth, S., & Oren, R. (2009). Leaf stomatal responses to vapour pressure deficit under current and CO_2-enriched atmosphere explained by the economics of gas exchange. *Plant, Cell and Environment*, *32*(8), 968–979. https://doi.org/10.1111/j.1365-3040.2009.01977.x

Keeling, C. D., Bacastow, R. B., Bainbridge, A. E., Ekdahl, C. A., Jr., Guenther, P. R., Waterman, L. S., & Chin, J. F. S. (1976). Atmospheric carbon dioxide variations at Mauna Loa observatory, Hawaii. *Tellus*, *28*(6), 538–551. https://doi.org/10.3402/tellusa.v28i6.11322

Knauer, J., Cuntz, M., Smith, B., Canadell, J. G., Medlyn, B. E., Bennett, A. C., et al. (2023). Higher global gross primary productivity under future climate with more advanced representations of photosynthesis. *Science Advances*, *9*(46), eadh9444. https://doi.org/10.1126/sciadv.adh9444

Knauer, J., Zaehle, S., Medlyn, B. E., Reichstein, M., Williams, C. A., Migliavacca, M., et al. (2018). Towards physiologically meaningful water-use efficiency estimates from eddy covariance data. *Global Change Biology*, *24*(2), 694–710. https://doi.org/10.1111/gcb.13893

Knorr, W. (2000). Annual and interannual CO_2 exchanges of the terrestrial biosphere: Process-based simulations and uncertainties. *Global Ecology and Biogeography*, *9*(3), 225–252. https://doi.org/10.1046/j.1365-2699.2000.00159.x

Konings, A. G., & Gentine, P. (2017). Global variations in ecosystem-scale isohydricity. *Global Change Biology*, *23*(2), 891–905. https://doi.org/10.1111/gcb.13389

Kumarathunge, D. P., Medlyn, B. E., Drake, J. E., Tjoelker, M. G., Aspinwall, M. J., Battaglia, M., et al. (2019). Acclimation and adaptation components of the temperature dependence of plant photosynthesis at the global scale. *New Phytologist*, *222*(2), 768–784. https://doi.org/10.1111/nph.15668

Lai, J., Kooijmans, L. M. J., Sun, W., Lombardozzi, D., Campbell, J. E., Gu, L., et al. (2024). Terrestrial photosynthesis inferred from plant carbonyl sulfide uptake. *Nature*, *634*(8035), 855–861. https://doi.org/10.1038/s41586-024-08050-3

Lawrence, D. M., Fisher, R. A., Koven, C. D., Oleson, K. W., Swenson, S. C., Bonan, G., et al. (2019). The community land model version 5: Description of new features, benchmarking, and impact of forcing uncertainty. *Journal of Advances in Modeling Earth Systems*, *11*(12), 4245–4287. https://doi.org/10.1029/2018ms001583

Leuning, R. (2002). Temperature dependence of two parameters in a photosynthesis model. *Plant, Cell and Environment*, *25*(9), 1205–1210. https://doi.org/10.1046/j.1365-3040.2002.00898.x

Li, H., Zhang, J., Zhang, S., & Bai, Y. (2022). Machine learning and remote sensing-based modeling of the optimal stomatal behavior of crops. *Computers and Electronics in Agriculture*, *200*, 107261. https://doi.org/10.1016/j.compag.2022.107261

Liang, W., Chen, Y., Fang, G., & Kaldybayev, A. (2023). Machine learning method is an alternative for the hydrological model in an alpine catchment in the Tianshan region, Central Asia. *Journal of Hydrology: Regional Studies*, *49*, 101492. https://doi.org/10.1016/j.ejrh.2023.101492

Lin, Y.-S., Medlyn, B. E., Duursma, R. A., Prentice, I. C., Wang, H., Baig, S., et al. (2015). Optimal stomatal behaviour around the world. *Nature Climate Change*, *5*(5), 459–464. https://doi.org/10.1038/nclimate2550

Liu, J., Hughes, D., Rahmani, F., Lawson, K., & Shen, C. (2023). Evaluating a global soil moisture dataset from a multitask model (GSM3 v1.0) with potential applications for crop threats. *Geoscientific Model Development*, *16*(5), 1553–1567. https://doi.org/10.5194/gmd-16-1553-2023

Liu, J., Rahmani, F., Lawson, K., & Shen, C. (2022). A multiscale deep learning model for soil moisture integrating satellite and in situ data. *Geophysical Research Letters*, *49*(7), e2021GL096847. https://doi.org/10.1029/2021GL096847

Lombardozzi, D. L., Bonan, G. B., Smith, N. G., Dukes, J. S., & Fisher, R. A. (2015). Temperature acclimation of photosynthesis and respiration: A key uncertainty in the carbon cycle-climate feedback. *Geophysical Research Letters*, *42*(20), 8624–8631. https://doi.org/10.1002/2015GL065934

Luo, X., Keenan, T., Chen, J., Croft, H., Prentice, I., Smith, N., et al. (2021). Global variation in the fraction of leaf nitrogen allocated to photosynthesis. *Nature Communications*, *12*(1), 4866. https://doi.org/10.1038/s41467-021-25163-9

Luo, X., & Keenan, T. F. (2020). Global evidence for the acclimation of ecosystem photosynthesis to light. *Nature Ecology & Evolution*, *4*(10), 1351–1357. https://doi.org/10.1038/s41559-020-1258-7

Massoud, E. C., Xu, C., Fisher, R. A., Knox, R. G., Walker, A. P., Serbin, S. P., et al. (2019). Identification of key parameters controlling demographically structured vegetation dynamics in a land surface model: CLM4.5(FATES). *Geoscientific Model Development*, *12*(9), 4133–4164. https://doi.org/10.5194/gmd-12-4133-2019

Medlyn, B. E., Dreyer, E., Ellsworth, D., Forstreuter, M., Harley, P. C., Kirschbaum, M. U. F., et al. (2002). Temperature response of parameters of a biochemically based model of photosynthesis. II. A review of experimental data. *Plant, Cell and Environment*, *25*(9), 1167–1179. https://doi.org/10.1046/j.1365-3040.2002.00891.x

Medlyn, B. E., Duursma, R. A., Eamus, D., Ellsworth, D. S., Prentice, I. C., Barton, C. V. M., et al. (2011). Reconciling the optimal and empirical approaches to modelling stomatal conductance. *Global Change Biology*, *17*(6), 2134–2144. https://doi.org/10.1111/j.1365-2486.2010.02375.x

Miner, G. L., & Bauerle, W. L. (2017). Seasonal variability of the parameters of the Ball–Berry model of stomatal conductance in maize (Zea mays L.) and sunflower (Helianthus annuus L.) under well-watered and water-stressed conditions. *Plant, Cell and Environment*, *40*(9), 1874–1886. https://doi.org/10.1111/pce.12990

Misson, L., Panek, J. A., & Goldstein, A. H. (2004). A comparison of three approaches to modeling leaf gas exchange in annually drought-stressed ponderosa pine forests. *Tree Physiology*, *24*(5), 529–541. https://doi.org/10.1093/treephys/24.5.529

Moreno-Martínez, Á., Camps-Valls, G., Kattge, J., Robinson, N., Reichstein, M., van Bodegom, P., et al. (2018). A methodology to derive global maps of leaf traits using remote sensing and climate data. *Remote Sensing of Environment*, *218*, 69–88. https://doi.org/10.1016/j.rse.2018.09.006

Mott, K. A., & Parkhurst, D. F. (1991). Stomatal responses to humidity in air and helox. *Plant, Cell and Environment*, *14*(5), 509–515. https://doi.org/10.1111/j.1365-3040.1991.tb01521.x

Muñoz Sabater, J. (2019). ERA5-Land hourly data from 1950 to present [Dataset]. *Copernicus Climate Change Service (C3S) Climate Data Store (CDS)*. https://doi.org/10.24381/cds.e2161bac

Nijs, I., Behaeghe, T., & Impens, I. (1995). Leaf nitrogen content as a predictor of photosynthetic capacity in ambient and global change conditions. *Journal of Biogeography*, *22*(2/3), 177–183. https://doi.org/10.2307/2845908

Norby, R. J., & Zak, D. R. (2011). Ecological lessons from free-air CO_2 enrichment (FACE) experiments. *Annual Review of Ecology Evolution and Systematics*, *42*(2011), 181–203. https://doi.org/10.1146/annurev-ecolsys-102209-144647

Nowak, R. S., Ellsworth, D. S., & Smith, S. D. (2004). Functional responses of plants to elevated atmospheric CO_2– do photosynthetic and productivity data from FACE experiments support early predictions? *New Phytologist*, *162*(2), 253–280. https://doi.org/10.1111/j.1469-8137.2004.01033.x

Oleson, K., Lawrence, D., Bonan, G., Drewniak, B., Huang, M., Koven, C., et al. (2013). *Technical description of version 4.5 of the community land model (CLM)*. UCAR/NCAR. https://doi.org/10.5065/D6RR1W7M

Pandurangam, V., Sharma-Natu, P., Sreekanth, B., & Ghildiyal, M. C. (2006). Photosynthetic acclimation to elevated CO_2 in relation to Rubisco gene expression in three C3 species. *Indian Journal of Experimental Biology*, *44*(5), 408–415.

Parida, P. K., Eagan, S., Ramanujam, K., Sengodan, R., Uthandi, S., Ettiyagounder, P., & Rajagounder, R. (2024). Machine learning approaches for estimation of the fraction of absorbed photosynthetically active radiation and net photosynthesis rate of maize using multi-spectral sensor. *Heliyon*, *10*(13), e34117. https://doi.org/10.1016/j.heliyon.2024.e34117

Pastorello, G., Trotta, C., Canfora, E., Chu, H., Christianson, D., Cheah, Y.-W., et al. (2020). The FLUXNET2015 dataset and the ONEFlux processing pipeline for eddy covariance data. *Scientific Data*, *7*(1), 225. https://doi.org/10.1038/s41597-020-0534-3

Paszke, A., Gross, S., Chintala, S., Chanan, G., Yang, E., DeVito, Z., et al. (2017). Automatic differentiation in PyTorch. In *31st Conference on Neural Information Processing Systems (NIPS 2017)*. Retrieved from https://openreview.net/forum?id=BJJsrmfCZ

Paszke, A., Gross, S., Massa, F., Lerer, A., Bradbury, J., Chanan, G., et al. (2019). PyTorch: An imperative style, high-performance deep learning library. In H. Wallach, H. Larochelle, A. Beygelzimer, F. Alché-Buc, E. Fox, & R. Garnett (Eds.), *Advances in neural information processing systems 32* (pp. 8024–8035). Curran Associates, Inc. Retrieved from http://papers.neurips.cc/paper/9015-pytorch-an-imperative-style-high-performance-deep-learning-library.pdf

Peng, Y., Bloomfield, K. J., Cernusak, L. A., Domingues, T. F., & Colin Prentice, I. (2021). Global climate and nutrient controls of photosynthetic capacity. *Communications Biology*, *4*(1), 462. https://doi.org/10.1038/s42003-021-01985-7

Pietsch, S. A., & Hasenauer, H. (2009). Photosynthesis within large-scale ecosystem models. In A. Laisk, L. Nedbal, & Govindjee (Eds.), *Photosynthesis in silico: Understanding complexity from Molecules to ecosystems* (pp. 441–464). Springer. https://doi.org/10.1007/978-1-4020-9237-4_19

Qian, T., Elings, A., Dieleman, J. A., Gort, G., & Marcelis, L. F. M. (2012). Estimation of photosynthesis parameters for a modified Farquhar–von Caemmerer–Berry model using simultaneous estimation method and nonlinear mixed effects model. *Environmental and Experimental Botany*, *82*, 66–73. https://doi.org/10.1016/j.envexpbot.2012.03.014

Querejeta, J. I., Prieto, I., Armas, C., Casanoves, F., Diémé, J. S., Diouf, M., et al. (2022). Higher leaf nitrogen content is linked to tighter stomatal regulation of transpiration and more efficient water use across dryland trees. *New Phytologist*, *235*(4), 1351–1364. https://doi.org/10.1111/nph.18254

Raddatz, T., Reick, C., Knorr, W., Kattge, J., Roeckner, E., Schnur, R., et al. (2007). Will the tropical land biosphere dominate the climate—Carbon cycle feedback during the 21st century? *Climate Dynamics*, *29*(6), 565–574. https://doi.org/10.1007/s00382-007-0247-8

Reddy, A. R., Rasineni, G. K., & Raghavendra, A. S. (2010). The impact of global elevated CO_2 concentration on photosynthesis and plant productivity. *Current Science*, *99*(1), 46–57. http://www.jstor.org/stable/24108349

Reed, P. M., Hadka, D., Herman, J. D., Kasprzyk, J. R., & Kollat, J. B. (2012). Evolutionary multiobjective optimization in water resources: The past, present, and future. *Advances in Water Resources*, *51*, 438–456. https://doi.org/10.1016/j.advwatres.2012.01.005

Rogers, A. (2014). The use and misuse of V(c,max) in Earth System Models. *Photosynthesis Research*, *119*(1–2), 15–29. https://doi.org/10.1007/s11120-013-9818-1

Rogers, A., Serbin, S., Ely, K., Wu, J., Wolfe, B., Dickman, T., et al. (2022). Diurnal leaf gas exchange survey. Feb2016-May2016, PA-SLZ, PA-PNM: Panama. https://doi.org/10.15486/ngt/1411972

Rudin, C. (2019). Stop explaining black box machine learning models for high stakes decisions and use interpretable models instead. *Nature Machine Intelligence*, *1*(5), 206–215. https://doi.org/10.1038/s42256-019-0048-x

Shen, C. (2018). A transdisciplinary review of deep learning research and its relevance for water resources scientists. *Water Resources Research*, *54*(11), 8558–8593. https://doi.org/10.1029/2018WR022643

Shen, C., Appling, A. P., Gentine, P., Bandai, T., Gupta, H., Tartakovsky, A., et al. (2023). Differentiable modelling to unify machine learning and physical models for geosciences. *Nature Reviews Earth & Environment*, *4*(8), 552–567. https://doi.org/10.1038/s43017-023-00450-9

Smith, N. G., Keenan, T. F., Colin Prentice, I., Wang, H., Wright, I. J., Niinemets, Ü., et al. (2019). Global photosynthetic capacity is optimized to the environment. *Ecology Letters*, *22*(3), 506–517. https://doi.org/10.1111/ele.13210

Song, Y., Tsai, W.-P., Gluck, J., Rhoades, A., Zarzycki, C., McCrary, R., et al. (2024). LSTM-based data integration to improve snow water equivalent prediction and diagnose error sources. *Journal of Hydrometeorology*, *25*(1), 223–237. https://doi.org/10.1175/JHM-D-22-0220.1

Spafford, L., & MacDougall, A. H. (2021). Validation of terrestrial biogeochemistry in CMIP6 earth system models: A review. *Geoscientific Model Development*, *14*(9), 5863–5889. https://doi.org/10.5194/gmd-14-5863-2021

Su, Y., Zhu, G., Miao, Z., Feng, Q., & Chang, Z. (2009). Estimation of parameters of a biochemically based model of photosynthesis using a genetic algorithm. *Plant, Cell and Environment*, *32*(12), 1710–1723. https://doi.org/10.1111/j.1365-3040.2009.02036.x

The Matplotlib Development Team. (2023). Matplotlib: Visualization with Python (Version v3.8.0) [Computer software]. *Zenodo*. https://doi.org/10.5281/zenodo.8347255

Thornton, P. E., Running, S. W., & Hunt, E. R. (2005). *Biome-BGC: Terrestrial ecosystem process model, Version 4.1.1*. ORNL Distributed Active Archive Center. https://doi.org/10.3334/ORNLDAAC/805

Tsai, W.-P., Feng, D., Pan, M., Beck, H., Lawson, K., Yang, Y., et al. (2021). From calibration to parameter learning: Harnessing the scaling effects of big data in geoscientific modeling. *Nature Communications*, *12*(1), 5988. https://doi.org/10.1038/s41467-021-26107-z

Vrugt, J. A., Gupta, H. V., Bastidas, L. A., Bouten, W., & Sorooshian, S. (2003). Effective and efficient algorithm for multiobjective optimization of hydrologic models. *Water Resources Research*, *39*(8). https://doi.org/10.1029/2002WR001746

Walker, A. P., Quaife, T., van Bodegom, P. M., De Kauwe, M. G., Keenan, T. F., Joiner, J., et al. (2017). The impact of alternative trait-scaling hypotheses for the maximum photosynthetic carboxylation rate (V_{cmax}) on global gross primary production. *New Phytologist*, *215*(4), 1370–1386. https://doi.org/10.1111/nph.14623

Wang, H., Prentice, I. C., Keenan, T. F., Davis, T. W., Wright, I. J., Cornwell, W. K., et al. (2017). Towards a universal model for carbon dioxide uptake by plants. *Nature Plants*, *3*(9), 734–741. https://doi.org/10.1038/s41477-017-0006-8

Wang, S., Peng, H., Hu, Q., & Jiang, M. (2022). Analysis of runoff generation driving factors based on hydrological model and interpretable machine learning method. *Journal of Hydrology: Regional Studies*, *42*, 101139. https://doi.org/10.1016/j.ejrh.2022.101139

Wu, T., Zhang, W., Wu, S., Cheng, M., Qi, L., Shao, G., & Jiao, X. (2023). Retrieving rice (Oryza sativa L.) net photosynthetic rate from UAV multispectral images based on machine learning methods. *Frontiers in Plant Science*, *13*. https://doi.org/10.3389/fpls.2022.1088499

Xu, C., Christoffersen, B., Robbins, Z., Knox, R., Fisher, R. A., Chitra-Tarak, R., et al. (2023). Quantification of hydraulic trait control on plant hydrodynamics and risk of hydraulic failure within a demographic structured vegetation model in a tropical forest (FATES-HYDRO V1.0). *EGUsphere*, *2023*, 1–32. https://doi.org/10.5194/egusphere-2023-278

Yang, S., Yang, D., Chen, J., Santisirisomboon, J., Lu, W., & Zhao, B. (2020). A physical process and machine learning combined hydrological model for daily streamflow simulations of large watersheds with limited observation data. *Journal of Hydrology*, *590*, 125206. https://doi.org/10.1016/j.jhydrol.2020.125206

Zhang, X.-Y., Huang, Z., Su, X., Siu, A., Song, Y., Zhang, D., & Fang, Q. (2020). Machine learning models for net photosynthetic rate prediction using poplar leaf phenotype data. *PLoS One*, *15*(2), e0228645. https://doi.org/10.1371/journal.pone.0228645